Analysis of prediction methods for non-equilibrium internal flow condensation heat transfer

Zheng, Xiaosheng; Zhang, Ji; Ryhl Kærn, Martin; Haglind, Fredrik

Published in:
Applied Thermal Engineering

Link to article, DOI:
10.1016/j.applthermaleng.2023.122063

Publication date:
2024

Document Version
Publisher's PDF, also known as Version of record

Applied Thermal Engineering 239 (2024) 122063

Contents lists available at ScienceDirect

Applied Thermal Engineering

journal homepage: www.elsevier.com/locate/apthermeng

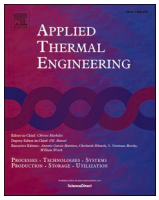

Research Paper

Analysis of prediction methods for non-equilibrium internal flow condensation heat transfer

Xiaosheng Zheng [a,*], Ji Zhang [b], Martin Ryhl Kærn [c], Fredrik Haglind [a]

[a] Department of Civil and Mechanical Engineering, Technical University of Denmark, Nils Koppels Allé, Building 403, 2800 Kongens Lyngby, Denmark
[b] College of Electrical and Information Engineering, Hunan University, Changsha 410082, China
[c] IPU, Bredevej 2B, 2830 Virum, Denmark

ARTICLE INFO

Keywords:
Non-equilibrium condensation
Prediction methods
Two-phase
Heat transfer mechanisms

ABSTRACT

Due to the climate crisis, there is a need to improve the performance of energy conversion systems and increase the use of renewable energy sources. In this context, accurate performance prediction methods for heat exchangers, including condensers, are of crucial importance. In the heat transfer process in a condenser including desuperheating and subcooling, both sensible and latent heat transfer may occur simultaneously due to thermal non-equilibrium effects. Liquid condensate may form close to the vapor saturation point of the bulk flow in the desuperheating region, while superheated vapor may penetrate beyond the liquid saturation point far into the two-phase region, and gas bubbles and subcooled mixture may exist in the subcooled region. These are complex phenomena that to a large extent affect the performance of the condenser. This paper presents an analysis of the prediction methods for non-equilibrium condensation heat transfer. First, the heat transfer mechanisms of non-equilibrium condensation are discussed. Next, state-of-the-art prediction methods developed for the target heat transfer processes are analyzed. Moreover, a database containing all data available in the open literature is built to evaluate the predictive performance of the prediction methods. Finally, a new prediction method is proposed for the subcooled condensation based on the identified heat transfer mechanisms. The results suggest that the Jacob correlation has the best predictive performance, followed by the Kondou correlation. The mean absolute percentage errors of both the Jacob and Kondou prediction methods are lower than 15 %, and more than 85 % of the experimental data points are predicted with a deviation within ± 30 %. The new prediction method proposed for the subcooled condensation is in good agreement with the experimental data, with a mean absolute percentage error of 12 %.

1. Introduction

With the rise of traditional energy prices [2] and concerns for the environment [3], utilizing the available energy sources in the most efficient manner and extending the use of renewable energy have become necessities. Thermal processes such as power generation systems, heat pump and refrigeration systems have gained worldwide acceptance as efficient ways to utilize low-temperature heat sources (e.g. solar, geothermal energy, and industry waste heat). In these thermal processes, the condenser serves as a critical component, and its heat transfer performance governs the performance of the energy conversion systems.

In practical applications, the condenser in thermal processes needs to be designed and operated with superheating (inlet) and subcooling degrees (outlet) apart from the two-phase region, for safety reasons and to ensure the operational performance of the other components (e.g. working fluid pump and expander). For example, in an organic Rankine cycle (ORC) process, subcooling is used to avoid cavitation that may cause oscillation and noise due to the presence of bubbles in the pump, while superheating is used to avoid two-phase flow in the expander [4]. For refrigeration systems, subcooling contributes to the improvement of the coefficient of performance, by increasing the cooling capacity [5]. However, almost all the existing methods used to predict the condensation heat transfer are based on the experimental results obtained from partial/completed condensation. The whole heat transfer process in the condenser was regarded as an equilibrium condensation process. Furthermore, the effects of inlet superheating and outlet subcooling were neglected when developing the prediction methods.

The occurrence of superheated vapor and subcooled liquid during

* Corresponding author.
E-mail address: xizhen@dtu.dk (X. Zheng).

https://doi.org/10.1016/j.applthermaleng.2023.122063
Received 28 August 2023; Received in revised form 7 November 2023; Accepted 17 November 2023
Available online 23 November 2023

Nomenclature

A	heat transfer area (m^2)
c_p	specific heat capacity ($kJ \cdot kg^{-1} \cdot K^{-1}$)
d	diameter (m)
d_h	hydraulic diameter (m)
e	wall thickness (m)
F	factor in Eq. (40) (–)
F_a	Petukov correction Factor (–)
f_b	friction factor (–)
g	acceleration of gravity ($m \cdot s^{-2}$)
G	mass flux ($kg \cdot m^{-2} \cdot s^{-1}$)
h	specific enthalpy ($kJ \cdot kg^{-1}$)
h_{lv}	latent heat of vaporization ($kJ \cdot kg^{-1}$)
J_G	dimensionless gas velocity (–)
J_G^T	transition dimensionless gas velocity (–)
K_i	correction factor of waviness (–)
l	heat transfer length (m)
m	mass flow rate ($kg \cdot s^{-1}$)
MAPE	mean absolute percentage error (%)
MPE	mean percentage error (%)
Nu	Nusselt number (–)
P	pressure (MPa)
Per	percentage (%)
Pr	Prandtl number (–)
q	heat flux ($W \cdot m^{-2}$)
Q	heat transfer rate (W)
Re	Reynolds number (–)
Re_{eq}	equivalent Reynolds number (–)
T	temperature (°C)
u	velocity ($m \cdot s^{-1}$)
U	global heat transfer coefficient ($W \cdot m^{-2} \cdot K^{-1}$)
x	thermodynamic quality (–)
x_{sup}	superficial thermodynamic quality (–)
X_{tt}	Lockhart-Martinelli parameter (–)

Greek Symbols

α	heat transfer coefficient ($W \cdot m^{-2} \cdot K^{-1}$)
δ	thickness of film (m)
ε	void fraction (–)
λ	thermal conductivity ($W \cdot m^{-1} \cdot K^{-1}$)
μ	dynamic viscosity ($kg \cdot m^{-1} \cdot s^{-1}$)
ρ	density ($kg \cdot m^{-3}$)
σ	surface tension ($N \cdot m^{-1}$)
ϕ	enlargement factor (–)
Δ	difference (–)

Subscript

annu	annular flow
AKERS	Akers et al. [1]
b	bulk flow
bubble	bubble temperature
con	condensation
dew	dew temperature
com	completion point of non-equilibrium condensation
exp	experiment
f	film
glide	temperature glide
i	inner
lam	laminar
lat	latent
lo	assumed liquid flow only
mix	zeotropic mixture
inc	Incipience point of non-equilibrium condensation
pre	prediction
r	refrigerant
sat	saturation
sens	sensible
strat	stratified flow
sub	subcool
sup	superheat
turb	turbulent
v	vapor
w	secondary fluid
wi	inner wall

Abbreviation

CSC	subcooled condensation
CSH	desuperheated condensation
HTC	heat transfer coefficient
ORC	organic Rankine cycle
PHE	plate heat exchanger
SBG	Silver, Bell and Ghaly method
TP	two-phase condensation

condensation heat transfer leads to the non-equilibrium phenomena. During condensation, the temperature profile across a cross-section in the flow channel typically is spatially non-uniform causing condensation to occur near the heat transfer wall where the wall temperature drops below the saturation vapor temperature, even though the bulk flow in the center of the channel is still superheated. Consequently, the condensation takes place before the saturation vapor point (thermodynamic quality x_b reaches 1), which is defined as desuperheated condensation (CSH). Similarly, condensation continues after the saturation liquid point (thermodynamic quality x_b is 0) due to the remaining vapor in the flow channel, which is defined as subcooled condensation (CSC). Moreover, the region between the saturation vapor point and the saturation liquid point is defined as saturated two-phase (TP) region. Fig. 1 presents the heat transfer processes of the non-equilibrium condensation. In this context, the concept of "condensation" is extended and defined as "non-equilibrium condensation" in this paper, considering non-equilibrium effects.

The existence of superheated vapor/subcooled liquid influences the heat transfer performance during condensation. Extensive literature has shown that superheated vapor has a positive impact on the heat transfer performance during condensation. Sarraf et al. [6] analyzed the enhancement of vapor superheat (from 5 °C to 25 °C) on the heat transfer coefficient (HTC) during condensation. They pointed out that the enhanced effect of the superheated vapor is particularly significant at low mass flux, resulting in a 70 % improvement in the HTC. Zhao et al. [7] experimentally investigated the effects of superheated vapor on the film condensation. Their experimental results suggest that the HTC of film condensation increases by 9.78 % when increasing the superheating degree from 39.5 K to 131.9 K. Longo et al. [8] compared the HTC of condensation with saturated vapor inlet and with superheated vapor inlet. They found that the HTCs of the latter are 8 % to 10 % higher than those of the former. Goto et al. [9] presented an HTC increase of around 5 % during condensation when increasing the inlet superheating degree from 0 K to 40 K.

Although the superheated vapor causes a positive impact to the whole non-equilibrium condensation, the effects of vapor (namely, latent heat transfer) in the CSC region are controversial. Jacob et al. [10] explored the effects of the subcooled liquid on the CSC region. They suggested that the enhancement due to latent heat transfer is limited and recommended to predict the HTC in the CSC region with a single-phase

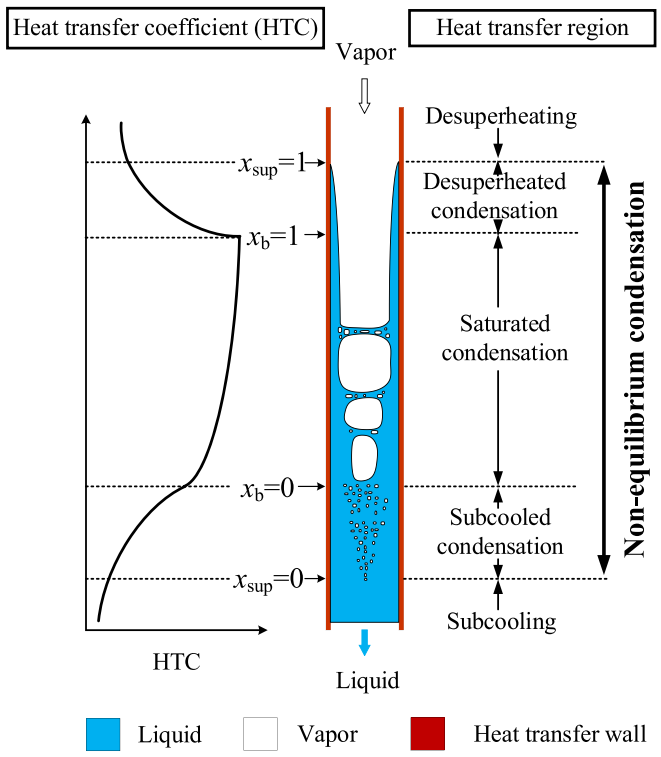

Fig. 1. The heat transfer process non-equilibrium condensation.

correlation. Kondou et al. [11] also ignored the latent heat transfer in the CSC region and simplified the model into fully sensible heat transfer. On the other hand, Agarwal et al. [12] considered the CSC as a developed latent heat transfer process and recommended to use two-phase heat transfer correlations for HTC prediction in this region. Based on the aforementioned literature, the heat transfer mechanisms in the CSC regions remain unclear, and there is a lack of tailored prediction methods for this heat transfer process.

Only a few previous studies focused specifically on the development of prediction methods for non-equilibrium condensation heat transfer. Agarwal et al. [12,13] proposed a unified model for non-equilibrium condensation, which bridges the discontinuity between single-phase and two-phase correlations. They pointed out that the existence of liquid in the CSH region and vapor in CSC region results in higher HTC. Their correlation predicts accurately the local HTC during the non-equilibrium condensation, with an absolute mean deviation of 16 %. Kondou et al. [11,14,15] measured the quasi-local HTC and demonstrated that condensation occurs before the saturation vapor point, and that the HTC in the desuperheated condensation region is significantly higher than the prediction results from single-phase correlations. By analyzing the temperature profile of the heat transfer wall, they also found that the CSH starts once the wall temperature drops below the saturation vapor temperature. They proposed two correlations for the CSH and TP regions, which are based on the properties of the condensate film. Xiao et al. [16,17] utilized flow visualization and film thickness measurement techniques to investigate the non-equilibrium condensation. They found that the HTC increases remarkedly in the CSH region and reaches a peak at the saturation vapor point. A unified model was proposed consisting of the non-equilibrium condensation region and single-phase region, which predicts the majority of data within a deviation range of ± 15 %. Longo et al. [8,18] conducted experiments of condensation with superheated vapor at the inlet port of a plate heat exchanger (PHE). They pointed out that the HTC of non-equilibrium condensation is 8 % to 10 % higher than that of saturated condensation, and recommended to use the Webb correlation [19] to predict the HTC in the CSH and TP regions.

This paper provides a first-of-its-kind comprehensive analysis of non-equilibrium condensation heat transfer. The governing heat transfer mechanisms are identified, and an evaluation of the predictive performance of the available heat transfer correlations for non-equilibrium condensation using all experimental data available in the open literature is carried out. Based on the evaluation of the state-of-the-art prediction methods, guidelines for the design of efficient condensers for thermal processes are presented. In addition, a new prediction method for subcooled condensation is developed. No previous work presents such a comprehensive evaluation including all existing heat transfer correlations applicable to non-equilibrium condensation and all experimental data available in the open literature. The analysis provides guidance for industry with respect to methods for designing condensers including subcooling and/or superheating, aiming at improving the performance of thermal processes and reducing the cost of heat transfer equipment. Furthermore, the research contributes to the academia by providing a comprehensive evaluation of the state-of-the-art prediction methods and a new prediction method for non-equilibrium condensation heat transfer.

The paper is divided into five sections. The heat transfer mechanisms of the target heat transfer processes are illustrated in Section 2, while Section 3 outlines the prediction methods, including an analysis of the essential parameters of the prediction methods. In Section 4, an evaluation of the predictive performance of the existing prediction methods for the CSH and CSC regions and new prediction method for the CSC region are presented. The conclusions are presented in Section 5.

2. Heat transfer mechanisms

Traditionally, the equilibrium theory assumes that condensation heat transfer starts when the thermodynamic quality of the bulk flow reaches 1, and ends at the position where the thermodynamic quality of the bulk flow is 0. There are three regions in a condenser: desuperheating, two-phase heat transfer, and subcooling. However, the assumptions of perfectly-mixed and fully-developed two-phase flow in equilibrium theory deviate from the reality in that the two-phase flow tends to be in non-equilibrium (e.g. non-homogenous distribution of temperature at a cross-section) during condensation. The non-equilibrium theory suggests that the condensation starts at the position where the wall temperature drops below the vapor saturation temperature, even though the bulk temperature of the working fluid is still above the saturation vapor temperature. In addition, the condensation continues after the bulk thermodynamic quality reaches zero. At this position, the majority of the working fluid is in the liquid phase, while there is still a small amount of vapor due to the uneven distribution of fluid temperature in a cross-section of the channel. The two-phase heat transfer is not completed until this part of the vapor is fully condensed.

Fig. 1 depicts the whole heat transfer process in a condenser considering the non-equilibrium effects. Initially, superheated vapor enters the desuperheating zone, releasing sensible heat. The working fluid is cooled down, while the wall temperature in the desuperheating region gradually declines. When the wall temperature becomes lower than the vapor saturation temperature, the superheated vapor close to the wall starts to condense, forming a liquid film. This region is called CSH, and in this region, the bulk fluid is in a desuperheated state. The traditional thermodynamic quality (x_b), which is determined by the bulk (average) temperature, is larger than 1 in the CSH region. However, the condensation (or two-phase) heat transfer is triggered in this region due to the non-equilibrium effects. For this reason, the “superficial quality” (x_{sup}) was introduced [16] based on the specific enthalpy, as shown in Eq. (16). The superficial quality of condensation incipience, the point where the wall temperature drops below the vapor saturation temperature, is artificially set to 1, while the superficial quality is set to 0 at the condensation completion, the point where the highest temperature of the working fluid in a cross-section of the channel drops below the liquid

saturation temperature. The CSH region continues until the bulk thermodynamic quality flow reaches 1. The heat transfer process consists of TP between the bulk thermodynamic quality of 1 and that of 0. At the position where the bulk thermodynamic quality reaches zero, the bulk (average) temperature of the fluid is equal to the liquid saturation temperature. However, the temperature of the fluid close to the wall is below the liquid saturation temperature, while that of the gas in the center of the heat transfer channel is larger. Thus, vapor still exists at the bulk thermodynamic quality of 0, and the condensation continues in the CSC zone until the highest temperature of the working fluid in a cross-section of the channel drops below the liquid saturation temperature. Finally, the liquid enters the subcooling region for further cooling. The whole heat transfer process of a condenser can be separated into five regions: desuperheating region, CSH region, TP region, CSC region and subcooling region, as shown in Fig. 1.

Fig. 2 presents a schematic of the heat transfer processes in the CSH and CSC regions, including the heat transfer paths, thermal resistances, and cross-sectional temperature profiles. The total heat transfer rate in the CSH region consists of the sensible (Q_{sens}) and latent (Q_{lat}) components, see Fig. 2(a). The bulk vapor in the core (central) region is cooled in a sensible heat transfer process. The driving temperature difference is governed by the bulk vapor temperature (T_b) and the inner surface temperature of the condensate film ($T_{v,sat}$), while the thermal resistance of the sensible heat transfer process (R_{sens}) is defined as the ratio of the driving temperature difference (T_b - $T_{v,sat}$) to the heat transfer rate (Q_{sens}). Moreover, due to the non-equilibrium effects, the superheated vapor close to the wall condenses and releases latent heat (Q_{lat}), which penetrates the condensate film to the wall. The driving temperature difference of the latent heat transfer depends on the inner surface temperature of the condensate film ($T_{v,sat}$) and the inner wall temperature (T_{wi}), and the thermal resistance of the latent heat transfer process (R_{lat}) is the ratio of the driving temperature difference ($T_{v,sat}$ - T_{wi}) to the heat transfer rate (Q_{lat}).

As for the CSC region, the total heat transfer rate is the combination of sensible (Q_{sens}) and latent (Q_{lat}) heat, as shown in Fig. 2(b). The bulk subcooled liquid is cooled in a sensible heat transfer process. The driving temperature difference is represented by (T_b - T_{wi}), while the thermal resistance of the sensible heat transfer process (R_{sens}) is the ratio of the driving temperature difference (T_b - T_{wi}) to the heat transfer rate (Q_{sens}). In addition, due to the non-equilibrium effects, there is vapor remaining in the center of the heat transfer channel that continues to condense, releasing latent heat. The driving temperature difference depends on the temperature of the remaining vapor ($T_{l,sat}$) and the bulk subcooled liquid temperature (T_b), and the thermal resistance of the latent heat transfer process (R_{lat}) is determined by the ratio of the driving temperature difference ($T_{l,sat}$ - T_b) to the heat transfer rate (Q_{lat}).

The effect of superheated vapor can be evaluated by comparing the average HTC of the CSH region with that in the TP region. The curve of HTC for the heat transfer process from superheated vapor to subcooled liquid is given in Fig. 3, which is based on the experimental data from Agarwal et al. [12]. In the beginning of the CSH region, the HTC sharply increases due to the occurrence of latent heat transfer. Afterwards, the HTC keeps increasing until it reaches the peak dominated by latent heat transfer. After that the flow enters the TP region and HTC starts to decrease due to the increase in heat transfer resistance of the condensed film. Therefore, the overall effect of the presence of superheated vapor at the inlet is governed by the competition between the average HTC of the CSH region ($\alpha_{ave,CSH}$) and the average HTC of the TP region ($\alpha_{ave,TP}$). If the average HTC of the CSH region is larger than that of the TP region, the superheated vapor has a positive effect on the non-equilibrium condensation. Otherwise, the superheated vapor will deteriorate the heat transfer. As shown in the CSH region of Fig. 3, the HTC decreases rapidly when increasing the degree of superheating, which leads to a lower $\alpha_{ave,CSH}$ (namely, $\alpha_{ave,CSH}$ significantly depends on the degree of superheating). Therefore, the heat transfer performance of a condenser can be improved by controlling the superheat degree at its inlet.

Compared to having superheated vapor at the condenser inlet, the effect of subcooled liquid on non-equilibrium condensation is relatively small. The reason is that the difference in HTC between two-phase and single-phase in the CSC region ($\Delta\ \alpha_{CSC}$) is small compared to that in the

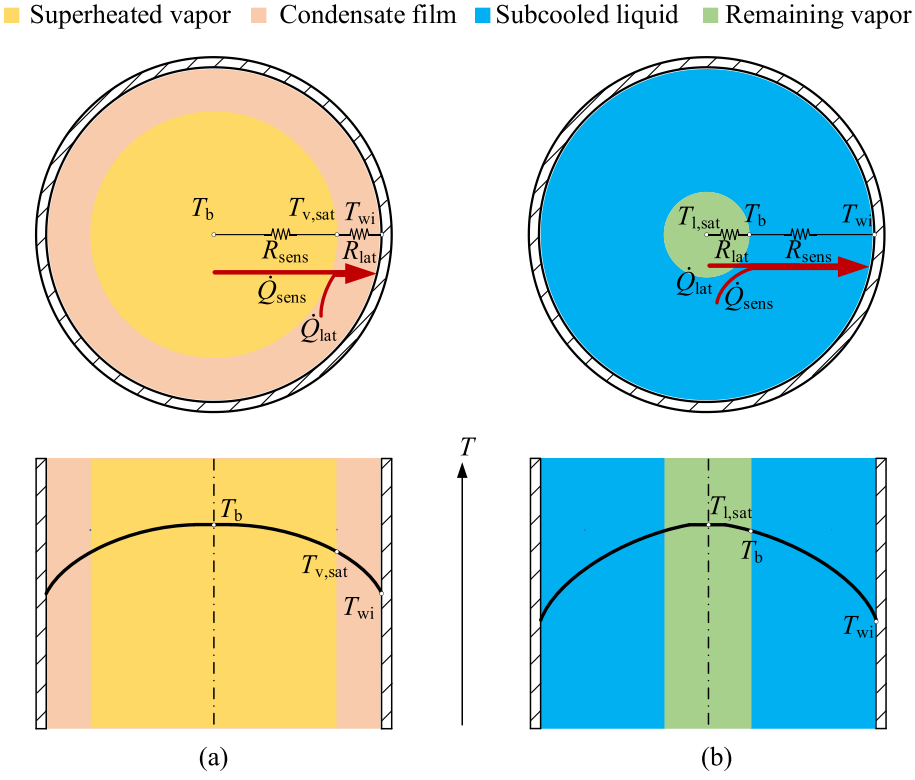

Fig. 2. Schematic of heat transfer processes during: (a) desuperheated condensation, (b) subcooled condensation.

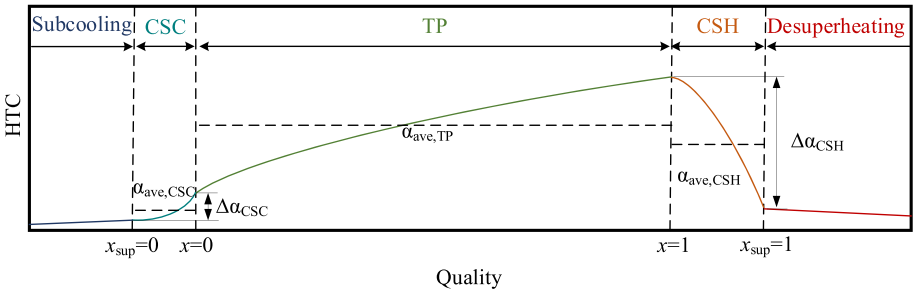

Fig. 3. HTC vs. quality along the whole heat transfer process in a condenser. The graph is obtained based on data from Agarwal et al. [12].

CSH region ($\Delta\ \alpha_{CSH}$), as shown in Fig. 3. This means the effect of two-phase heat transfer in the CSC region is limited [10]. In addition, it is challenging to determine the position of complete non-equilibrium condensation using existing methods. This is because the local heat flux and HTC at completion points, which should be obtained a priori, are unknown (see detailed analysis in Section 4.3). For these reasons, almost all the previous works considering non-equilibrium condensation focused on the heat transfer in the CSH region, rather than in the CSC region.

3. Prediction methods

Almost all previous research on condensation heat transfer focused on the development of prediction methods for equilibrium partial/completed condensation. However, the incipience and completion points of condensation change due to the non-equilibrium effects, which may influence the predictive performance of the prediction methods. In this section, the state-of-the-art prediction methods [8,10–12,16] available in the open literature for the heat transfer coefficient considering non-equilibrium effects are described. The selected prediction methods were specifically developed for non-equilibrium condensation, particularly for the CSH and CSC regions, where the traditional methods fail to provide accurate results. The prediction methods considered were developed for heat transfer, either in a tube or PHE using pure working fluids or zeotropic mixtures. In addition, a new prediction method for the CSC region is developed.

3.1. Agarwal correlation

Agarwal et al. [12] developed a unified correlation for the CSH, TP and CSC regions. The correlation is based on the heat transfer mechanism proposed by Webb et al. [19] and it is applicable for in-tube flow. Webb [19] defined superposition as implying that the heat flux in the CSH region (q_{CSH}) includes two components, sensible (q_{sens}) and latent heat flux (q_{lat}):

$$q_{CSH} = q_{sens} + q_{lat} \tag{1}$$

During the CSH heat transfer process, the bulk flow is cooled down from a superheated state, resulting in a declining superheat degree. The heat flux of the bulk flow is sensible heat flux, which is obtained by Eq. (2). Parameter α_{SH} is the HTC of the vapor phase, while T_b and $T_{v,sat}$ are the bulk and vapor saturation temperature of the working fluid. At the same time, the superheated vapor, which is in contact with the wall, will condense directly from superheated vapor to saturation liquid. The heat flux of the fluid is latent heat flux, which is given by Eq. (3). The α_{TP} is the HTC of saturation two-phase, while T_{wi} is the inner wall temperature of the heat transfer surface.

$$q_{sens} = \alpha_{SH}(T_b - T_{v,sat}) \tag{2}$$

$$q_{lat} = \alpha_{TP}(T_{v,sat} - T_{wi}) \tag{3}$$

$$q_{CSH} = \alpha_{CSH}(T_{v,sat} - T_{wi}) \tag{4}$$

The total heat flux (q_{CSH}) is calculated using Eq. (4), where α_{CSH} is the HTC of desuperheated condensation. Substituting Eqs. (2)-(4) into Eq. (1) gives the following:

$$\alpha_{CSH} = \left[\alpha_{SH}(T_b - T_{v,sat}) + \alpha_{TP}(T_{v,sat} - T_{wi})\right] / \left(T_{v,sat} - T_{wi}\right) \tag{5}$$

Agarwal et al. [12] evaluated the predictive performance of Webb's prediction method for the CSH region with their experimental data. Based on the results, they modified the heat transfer temperature difference of the total heat flux to (T_b - T_{wi}) and obtained the following equation:

$$\alpha_{CSH} = \left[\alpha_{SH}(T_b - T_{v,sat}) + \alpha_{TP}(T_{v,sat} - T_{wi})\right] / (T_b - T_{wi}) \tag{6}$$

In the equation, both single-phase and two-phase heat transfer are considered. Appropriate correlations for the superheated vapor and the saturation two-phase flow need to be determined. Agarwal et al. [12] suggested the Gnielinski correlation [20] and Cavallini correlation [21] for superheated vapor and saturation two-phase heat transfer, respectively. The Gnielinski correlation [20] was developed for the single-phase flow considering the friction factor f_b of the heat transfer surface. The correlation is applicable only for turbulent flow ($Re > 10^4$), and it reads as follows:

$$\left.\begin{aligned} \alpha_{SH} &= \frac{(f_b/8)(G_v d_i/\mu_v - 1000)Pr_v}{1 + 12.7(f_b/8)^{1/2}\left(Pr_v^{2/3} - 1\right)}(\lambda_v/d_i) \\ f_b &= \left[1.82\log_{10}(G_v d_i/\mu_v) - 1.64\right]^{-2} \end{aligned}\right\} \tag{7}$$

where G_v, μ_v, Pr_v, and λ_v are the mass flow rate, dynamic viscosity, Prandtl number and thermal conductivity of the superheated vapor, respectively. d_i represents the inner diameter of the tube.

The Cavallini correlation [21] has been extensively applied and comprehensively validated using experimental data for saturation two-phase heat transfer. Cavallini et al. [21] divided the whole saturation two-phase heat transfer process into two parts, a ΔT-dependent and a ΔT-independent flow regime (ΔT indicates the temperature difference between the saturation temperature and the wall temperature).The transition dimensionless gas velocity J_G^T and dimensionless gas velocity J_G are used to determine the transition line between the ΔT-dependent and ΔT-independent flow regimes. The prediction method for the TP region is shown in the following:

ΔT-independent regime ($J_G > J_G^T$):

$$\alpha_{TP,1} = \alpha_{annu} = \alpha_{lo}\left[1 + 1.128x_b^{0.817}\left(\frac{\rho_l}{\rho_v}\right)^{0.3685}\left(\frac{\mu_l}{\mu_v}\right)^{0.2363}\left(1 - \frac{\mu_v}{\mu_l}\right)^{2.144} Pr_l^{-0.1}\right] \tag{8}$$

$$\alpha_{lo} = 0.023(Gd_i/\mu_l)^{0.8} Pr_l^{0.4}(\lambda_l/d_i) \tag{9}$$

ΔT-dependent regime ($J_G < J_G^T$):

$$\alpha_{TP,2} = \left[\alpha_{annu}\left(J_G^T/J_G\right)^{0.8} - \alpha_{strat}\right]\left(J_G/J_G^T\right) + \alpha_{strat} \tag{10}$$

$$\alpha_{strat}=0.725\left[\frac{\lambda_l^3\rho_l(\rho_l-\rho_v)g\Delta h_{lv}}{\mu_l d_i(T_{sat}-T_w)}\right]^{0.25}\left\{1+0.741\left(\frac{1-x_b}{x_b}\right)^{0.3321}\right\}^{-1}+\left(1-x_b^{0.087}\right)\alpha_{lo} \tag{11}$$

where J_G and J_G^T are obtained by Eq. (12):

$$\left.\begin{aligned} J_G^T&=\left\{\left[7.5/\left(4.3X_{tt}^{1.111}+1\right)\right]^{-3}+2.6^{-3}\right\}^{-1/3}\\ J_G&=\frac{x_bG}{\left[gd_i\rho_v(\rho_l-\rho_v)\right]^{0.5}}\\ X_{tt}&=\left(\frac{\mu_l}{\mu_v}\right)^{0.1}\left(\frac{\rho_v}{\rho_l}\right)^{0.5}\left[\frac{(1-x_b)}{x_b}\right]^{0.9}\end{aligned}\right\} \tag{12}$$

where $\alpha_{TP,1}$ and $\alpha_{TP,2}$ represent the HTC in the Δ T-independent and Δ T-dependent regions, respectively. Parameters α_{auua}, α_{lo} and α_{strat} are the HTC of annual flow, assumed only liquid flow, and stratified flow, respectively. ρ, g, Δ h_{lv}, and X_{tt} indicate density, acceleration of gravity, latent heat of vaporization, and the turbulent-turbulent Lockhart-Martinelli parameter, respectively. When calculating the HTC of the latent heat transfer ($\alpha_{TP,1}$ and $\alpha_{TP,2}$) during the CSH process, Agarwal et al. [12] assumed that the thermodynamic quality x_b is equal to 0.9999. All the properties of the liquid (with subscript l) and vapor (with subscript v) are taken as saturated and superheated states, respectively.

As for the prediction method for the saturation two-phase process, Eqs. (8) - (12) are used directly, with the properties of liquid and vapor taken as the saturation condition. x_b is the bulk thermodynamic quality, which is determined by enthalpy and pressure. The CSC region is combined with the TP region, and the same equations are used to calculate the HTC in this region. The inlet thermodynamic quality of the working fluid in the CSC region is taken as the outlet thermodynamic quality of the last segment of the TP region.

3.2. Kondou correlation

Kondou et al. [11] developed a consolidated correlation for the CSH and TP regions, which is applicable for in-tube flow. Eq. (6) was utilized to calculate the HTC in the CSH region. However, different correlations for superheated vapor and saturation two-phase flow were selected. For the single-phase correlation, the Petukov [22] correction Factor F_a was introduced, on the basis of the Gnielinski correlation [20]:

$$\left.\begin{aligned}\alpha_{SH}&=\frac{(f_b/8)(G_vd_i/\mu_v-1000)Pr_v}{1+12.7(f_b/8)^{1/2}\left(Pr_v^{2/3}-1\right)}F_a(\lambda_v/d_i)\\ Fa&=\left(\frac{T_{wi}}{T_b}\right)^{-0.36}\end{aligned}\right\} \tag{13}$$

The saturation two-phase condensation in the CSH region was computed using Eqs. (14) and (15). The film temperature (T_f) was introduced to determine the thermodynamic properties (with the subscript f). Kondou et al. [11] assumed that the x_b in the CSH region is set to 0.995. All the properties of the liquid (with subscript l) and the vapor (with subscript v) were taken as saturated and superheated states, respectively.

Δ T-independent regime ($J_G > J_G^T$):

$$\left.\begin{aligned}\alpha_{TP,1}&=\alpha_{lo\_f}\left[1+1.128x_b^{0.817}\left(\frac{\rho_l}{\rho_v}\right)^{0.3685}\left(\frac{\mu_l}{\mu_v}\right)^{0.2363}\left(1-\frac{\mu_v}{\mu_l}\right)^{2.144}Pr_{l\_f}^{-0.1}\right]\\ \alpha_{lo\_f}&=0.023\left(Gd_i/\mu_{l\_f}\right)^{0.8}Pr_{l\_f}^{0.4}(\lambda_l/d_i)\end{aligned}\right\} \tag{14}$$

Δ T-dependent regime ($J_G < J_G^T$):

$$\left.\begin{aligned}\alpha_{TP,2}&=\left[\alpha_{TP,1}\left(J_G^T/J_G\right)^{0.8}-\alpha_{strat}\right]\left(J_G/J_G^T\right)+\alpha_{strat}\\ T_f&=\frac{T_{wi}+T_{sat}}{2}\\ Pr_{l\_f}&=\left(c_{pl}\mu_{l\_f}\right)/\lambda_{l\_f}\\ c_{pl}&=\left(h_l-h_{l,wi}\right)/\left(T_{sat}-T_{wi}\right)\\ \alpha_{strat}&=0.725\left[\frac{\lambda_{l\_f}^3\rho_{l\_f}\left(\rho_{l\_f}-\rho_v\right)g\Delta h_{lv}}{\mu_{l\_f}d_i(T_{sat}-T_{wi})}\right]^{0.25}\left\{1+0.741\left(\frac{1-x_b}{x_b}\right)^{0.3321}\right\}^{-1}+\left(1-x_b^{0.087}\right)\alpha_{lo\_f}\end{aligned}\right\} \tag{15}$$

where c_{pl} and $h_{l,wi}$ are the average specific heat capacity of saturation liquid and enthalpy determined by inner wall temperature as well as condensation pressure, respectively. When it comes to the TP region, Eq. (14) and Eq. (15) were used. The properties of the liquid and vapor were taken as saturation conditions. The thermodynamic quality of the bulk flow is the actual value, which is determined by enthalpy and pressure.

3.3. Xiao correlation

Xiao et al. [16] proposed a heat transfer model for in-tube flow accounting for non-equilibrium effects. The superficial thermodynamic quality x_{sup}, which is used to rescale the thermodynamic quality for non-equilibrium condensation, was introduced:

$$x_{sup}=\frac{h-h_{com}}{h_{inc}-h_{com}} \tag{16}$$

where h, h_{com} and h_{inc} represent the local enthalpy, the enthalpy at the incipience point and at the completion point of non-equilibrium condensation, respectively. In order to obtain h_{com} and h_{inc}, first the temperature at the incipience point and completion point need to be determined:

$$T_{inc}=T_{v,sat}+\frac{q_{inc}}{\alpha_{inc}} \tag{17}$$

$$T_{com}=T_{l,sat}-\frac{q_{com}}{\alpha_{com}} \tag{18}$$

where the q is the heat flux at the incipience/completion point, while α_{inc} and α_{com} represent the HTC at the incipience and completion points, respectively. α_{inc} and α_{com} can be determined by appropriate single-phase correlations (e.g. the Dittus-Boelter equation [23] or Gnielinski correlation [20]). Eq. (18) is based on the assumption of a developed laminar flow right after the end of the condensation. However, in practice, the flow may be turbulent, and not laminar. For this reason, a correction factor 0.33 is introduced to increase the prediction accuracy of the completion point:

$$T_{com}=T_{l,sat}-0.33\frac{q_{com}}{\alpha_{com}} \tag{19}$$

Xiao et al. [16] separated the non-equilibrium condensation process into annular flow and stratified flow. For the annular flow, the model was developed based on the Dittus-Boelter equation [23], by replacing the liquid Reynolds number (Re_l) with the film Reynolds number (Re_f). The ratio of the radius ($d_i/2$) to the film thickness (δ) was introduced to reflect the effect of film thickness on the HTC (the thinner the liquid film, the higher the HTC). Another correction factor, K_i, was introduced to consider the effect of interfacial waviness and liquid entrainment. The correlation for annular flow is shown in the following:

$$\alpha_{f,annu}=0.023Re_f^{0.8}Pr_l^{0.3}\frac{\lambda_l}{d_i}\left(\frac{d_i}{2\delta}\right)^{0.94}\frac{T_{b,l}-T_{wi}}{T_{sat}-T_{wi}}K_i \tag{20}$$

$$\left.\begin{aligned} Re_f &= \left[2G\left(1-x_{\text{sup}}\right)\delta\right]/\left[(1-\varepsilon)\mu_l\right] \\ \delta &= 0.5d_i - 0.5\left(d_i^2 - 4A_l/\pi\right)^{0.5} \\ A_l &= \left[\pi d_i^2(1-\varepsilon)\right]/4 \end{aligned}\right\} \tag{21}$$

$$\left.\begin{aligned} \varepsilon_{\text{homo}} &= \left[1+\left(\frac{1-x_{\text{sup}}}{x_{\text{sup}}}\right)\left(\frac{\rho_v}{\rho_l}\right)\right]^{-1} \\ \varepsilon_{ra} &= \frac{x_{\text{sup}}}{\rho_v}\left[\begin{aligned} &1+0.12\left(1-x_{\text{sup}}\right)\left(\frac{x_{\text{sup}}}{\rho_v}+\frac{1-x_{\text{sup}}}{\rho_l}\right) \\ &+\frac{1.18\left(1-x_{\text{sup}}\right)\left[g\sigma(\rho_l-\rho_v)\right]^{0.25}}{G\rho_l^{0.5}} \end{aligned}\right]^{-1} \\ \varepsilon &= \frac{\varepsilon_{\text{homo}}-\varepsilon_{ra}}{In\left(\frac{\varepsilon_{\text{homo}}}{\varepsilon_{ra}}\right)} \end{aligned}\right\} \tag{22}$$

$$K_i = 1+\left(\frac{u_v}{u_l}\right)^{0.5}\left[\frac{(\rho_l-\rho_v)g\delta^2}{\sigma}\right]^{0.34}x_{\text{sup}}^{0.1} \tag{23}$$

where $\alpha_{f,annu}$ is the HTC for annular flow. The parameters σ, ε and A_l represent surface tension, void fraction, and cross-sectional profile of the film, respectively. For the purpose of simplicity of the model, the bulk liquid temperature ($T_{b,l}$) is set to vapor saturation temperature ($T_{v,sat}$) in the CSH region, to saturation temperature (T_{sat}) in the TP region, and to bulk flow temperature (T_b) in the CSC region.

In terms of the stratified flow, the tube is divided into the upper part (with constant film thickness) and the lower part (with varying film thickness). The HTCs of the upper part ($\alpha_{f,upper}$) and lower part ($\alpha_{f,lower}$) are combined to determine the total HTC ($\alpha_{f,strat}$) of stratified flow. Following is the correlation for stratified flow:

$$A_l = \frac{d_i^2}{8}\left[(2\pi-\theta_{strat})-\sin(2\pi-\theta_{strat})+\theta_{strat}(1-\varepsilon_{trans})\right] \tag{24}$$

$$\delta_{lower} = 0.5d_i\left[1-\frac{\sin(2\pi-\theta_{strat})}{2\pi-\theta_{strat}}\right] \tag{25}$$

$$Re_{f,lower} = \left[2G\left(1-x_{\text{sup}}\right)\delta_{lower}\right]/\left[(1-\varepsilon)\mu_f\right] \tag{26}$$

$$Re_{f,upper} = \left[2G\left(1-x_{\text{sup}}\right)\delta_{trans}\right]/\left[(1-\varepsilon)\mu_f\right] \tag{27}$$

$$\alpha_{f,lower} = 0.023Re_{f,lower}^{0.8}Pr_l^{0.3}\frac{\lambda_l}{d_i}\left(\frac{d_i}{2\delta_{lower}}\right)^{0.94}\frac{T_{b,l}-T_{wi}}{T_{sat}-T_{wi}}K_i \tag{28}$$

$$\alpha_{f,upper} = 0.023Re_{f,upper}^{0.8}Pr_l^{0.3}\frac{\lambda_l}{d_i}\left(\frac{d_i}{2\delta_{trans}}\right)^{0.94}\frac{T_{b,l}-T_{wi}}{T_{sat}-T_{wi}}K_i \tag{29}$$

$$\alpha_{f,strat} = \alpha_{f,upper}\frac{\theta_{strat}}{2\pi}+\alpha_{f,lower}\frac{2\pi-\theta_{strat}}{2\pi} \tag{30}$$

where θ_{strat}, ε_{trans} and δ_{trans} indicate the stratification angle, as well as void fraction and film thickness at the transition between annual and stratified flow, respectively. δ_{lower} and $Re_{f,lower}$ represent the film thickness and Reynolds number of the lower part, while $Re_{f,upper}$ is the Reynolds number of the upper part.

The current model introduced the film HTC ($\alpha_{f,annu/strat}$) as a tool to model the non-equilibrium condensation. It is significantly important to convert it back to the bulk HTC ($\alpha_{CSH/TP/CSC}$). The following conversion equation is shown for the CSH, TP and CSC regions:

$$\alpha_{CSH/TP/CSC} = \frac{T_{sat}-T_{wi}}{T_b-T_{wi}}\alpha_{f,annu/strat} \tag{31}$$

In order to simplify the model, Xiao et al. [16] regarded the whole non-equilibrium condensation process as annual flow and used the corresponding correlations (Eqs. (20) - (23)) to calculate the film HTC. The conversion HTCs in each region are simplified as follows:

CSH region:

$$\alpha_{CSH} = 0.023Re_f^{0.8}Pr_l^{0.3}\frac{\lambda_l}{d_i}\left(\frac{d_i}{2\delta}\right)^{0.94}\frac{T_{v,sat}-T_{wi}}{T_b-T_{wi}}K_i \tag{32}$$

TP and CSC regions:

$$\alpha_{TP/CSC} = 0.023Re_f^{0.8}Pr_l^{0.3}\frac{\lambda_l}{d_i}\left(\frac{d_i}{2\delta}\right)^{0.94}K_i \tag{33}$$

where α_{CSH} is the HTC for the CSH region and $\alpha_{TP/CSC}$ is for the TP or CSC region.

3.4. Jacob correlation

Jacob et al. [10] investigated the non-equilibrium condensation of zeotropic mixtures and developed a new prediction method considering the mixtures effects. The Jacob correlation is applicable for in-tube flow. The equilibrium SBG [24,25] method was utilized to calculate the HTC for mixtures:

$$\alpha_{mix} = \left[\frac{1}{\alpha_{\text{model}}}+\frac{x_{\text{sup}}c_{p,v}(T_{dew}-T_{bubble})}{\Delta h_{lv}}\frac{1}{\alpha_v}\right]^{-1} \tag{34}$$

where α_{model} represents the HTC of the CSH or TP regions, while T_{dew}, T_{bubble} and α_v are the dew point temperature, bubble point temperature, and HTC of the vapor, respectively. The HTC of the CSH region can be obtained by Eq.(35), while that of the TP region can be obtained using Eqs. (8) - (12). In Eq. (35), q_{total} represents the local heat flux in the CSH region. The bulk thermodynamic quality was replaced by the superficial thermodynamic quality x_{sup}, given by Eq. (36). The enthalpy of the incipience point of non-equilibrium condensation can be determined by Eq. (17) and the local pressure.

$$\alpha_{CSH} = \left[\frac{1}{\alpha_{TP}}+\frac{T_v-T_{dew}}{q_{total}}\right]^{-1} \tag{35}$$

$$x_{\text{sup}} = \frac{h_b-h_{l,sat}}{h_{onset}-h_{l,sat}} \tag{36}$$

Jacob et al. [10] neglected the enhancement of the latent effect in the CSC region and regarded it as a subcooling region, which was predicted using the Gnielinski prediction method [20]. The single-phase HTC in the turbulent region ($Re > 10^4$) is calculated by Eq. (7), while that in the laminar and transition regions (α_l) can be obtained by the following equations:

Laminar region ($Re < 2300$):

Constant wall temperature:

$$\left.\begin{aligned} \alpha_l &= \frac{\lambda_l}{d}\left[Nu_{m,T,1}^3+0.7^3+\left(Nu_{m,T,2}-0.7\right)^3+Nu_{m,T,3}^3\right]^{1/3} \\ Nu_{m,T,1} &= 3.66 \\ Nu_{m,T,2} &= 1.615[RePr(d_i/l)]^{1/3} \\ Nu_{m,T,3} &= \left(\frac{2}{1+22Pr}\right)^{1/6}[RePr(d_i/l)]^{1/2} \end{aligned}\right\} \tag{37}$$

Constant heat flux:

$$\left.\begin{aligned} \alpha_l &= \frac{\lambda_l}{d}\left[Nu_{m,q,1}^3+0.6^3+\left(Nu_{m,q,2}-0.6\right)^3\right]^{1/3} \\ Nu_{m,q,1} &= 4.364 \\ Nu_{m,q,2} &= 1.953[RePr(d_i/l)]^{1/3} \end{aligned}\right\} \tag{38}$$

Transition region ($2300 < Re < 10^4$):

$$\left.\begin{aligned} \alpha_l &= \frac{\lambda_l}{d_i}\left[(1-\gamma)Nu_{lam,2300} + \gamma Nu_{turb,10^4}\right] \\ \gamma &= \frac{Re-2300}{10^4-2300} \end{aligned}\right\} \tag{39}$$

where $Nu_{m,T,1}$, $Nu_{m,T,2}$ and $Nu_{m,T,3}$ represent the first, second and third Nusselt number at constant wall temperature, respectively. $Nu_{m,q,1}$ and $Nu_{m,q,2}$ indicate the first and second Nusselt number at constant heat flux, respectively. $Nu_{lam,2300}$ and $Nu_{turb,10^4}$ are the Nusselt number for laminar and turbulent flow, respectively. The parameters l and γ represent the length of the tube and proportion of turbulent flow, respectively.

3.5. Longo correlation

Longo et al. [8] conducted experiments to validate the prediction method by Webb [19], which was used to predict the HTC for the CSH and TP regions in PHEs. The Longo correlation was developed for the flow in PHEs. Longo et al. [8] suggested using the correlation by Akers et al. [1] for the saturation TP region and the Thonon et al. [26] equation for the single-phase region:

$$\left.\begin{aligned} \alpha_{CSH} &= \alpha_{TP} + F\left[\alpha_{SH} + c_{p,v}q_{lat}/\Delta h_{lv}\right] \\ \alpha_{TP} &= \phi\alpha_{AKERS} \\ \alpha_{AKERS} &= 5.03\left(\lambda_{l,sat}/d_h\right)Re_{eq}^{1/3}Pr_{l,sat}^{1/3} \\ Re_{eq} &= G\left[(1-x_b) + x_b\left(\rho_{l,sat}/\rho_{v,sat}\right)^{1/2}\right]\left(d_h/\mu_{l,sat}\right) \\ \alpha_{SH} &= 0.2267(\lambda_v/d_h)Re_v^{0.631}Pr_v^{1/3} \\ F &= (T_b - T_{v,sat})/(T_b - T_{wi}) \\ q_{lat} &= \alpha_{TP}\left(T_{v,sat} - T_{wi}\right) \end{aligned}\right\} \tag{40}$$

where F is the ratio of the local superheat degree to the driving temperature difference. ϕ, Re_{eq} and α_{AKERS} represent the enlargement factor, the equivalent Reynolds number and the HTC obtained using the Akers correlation [1], respectively.

3.6. Basic format and critical parameters

In this section, the aforementioned prediction methods for non-equilibrium condensation are summarized and analyzed. A majority of the prediction methods for the CSH region use the Webb correlation [19] as the basic format. The HTC of both the vapor phase (α_{SH}) and the saturation two-phase (α_{TP}) are combined into the prediction method. Thus, the correlation is based on both the sensible heat transfer resulting from the cooling process and latent heat transfer resulting from the condensation process. Some of the prediction methods for the CSH region are based on the film theory, taking the Dittus-Boelter equation as the basic format. As for the prediction methods for zeotropic mixtures, the equilibrium SBG [24,25] method is utilized as the basic format, considering the mixture effects. For these prediction methods, the HTC of the single-phase heat transfer is mainly obtained by the Gnielinski prediction method [20] or the Dittus-Boelter equation [23], while the HTC of the two-phase heat transfer is calculated using the Cavallini prediction method [21] or Akers correlation [1].

As for prediction methods for the TP region, the Cavallini prediction method [21] is widely used. However, depending on different heat transfer mechanisms, different characteristic temperatures will be considered (bulk or film temperature). In order to adapt the method to different applications, a series of correction terms considering mass transfer, mixture effects and/or waviness effect are added. In addition, some prediction methods for the CSH region take the Dittus-Boelter equation [23] as the basic format, which is based on the film theory.

As for the CSC region, the same prediction methods as those used for the TP region are used since the same heat transfer mechanisms occur in these regions. Some researchers tend to neglect this region and regard it as a subcooling region, since the enhancement effect of the two-phase heat transfer in the CSC region is limited.

An overview of the crucial dimensionless numbers, thermodynamic properties and applications of the different prediction methods under consideration are provided in Table 1, while Fig. 4(a) - (b) depicts the frequency of these key parameters. The results suggest that the Reynolds number and Prandtl number are the dominating parameters regarding the dimensionless number. As for the thermodynamic properties, the superheat degree (ΔT_{sup}) and subcooling degree of the wall ($\Delta T_{sub,w}$) are introduced into the prediction methods, considering the effect of superheated vapor and secondary fluids. Density, viscosity and thermal conductivity at saturation vapor and liquid states are commonly used. In addition, the superficial thermodynamic quality (x_{sup}) is utilized to rescale the quality to cover the whole non-equilibrium condensation process. For zeotropic mixtures, the temperature glide (ΔT_{glide}), the specific heat capacity of the vapor phase ($c_{p,v}$), and the enthalpy difference between saturation liquid and vapor (Δh_{lv}) are introduced to take the mixture effects into account.

3.7. New prediction method

For the CSC region, the governed heat transfer mechanisms are unclear. Therefore, a new prediction method is proposed for this region. The new prediction method is based on the coexistence of the sensible (single-phase) and latent (two-phase) heat transfer mechanisms in the CSC region. In this region, the liquid bulk fluid is governed by sensible heat transfer, while the remaining vapor primarily is governed by latent heat transfer. Therefore, the HTC of the CSC (α_{CSC}) is combined by the HTC of the sensible heat transfer (α_{SP}) and that of the latent heat transfer (α_{TP}), considering the sensible component and latent component, respectively. Moreover, two correction factors are introduced to scale the contributions of the sensible heat transfer (F_{SP}) and the latent heat transfer (F_{TP}). The correlation reads as follows:

$$\alpha_{CSC} = F_{SP}\cdot\alpha_{SP} + F_{TP}\cdot\alpha_{TP} \tag{41}$$

The Dittus-Boelter equation [23], Eq. (42), is used to compute the sensible HTC (α_{SP}), while the Cavallini correlation [21], Eqs. (8)-(12), is used to obtain the latent HTC (α_{TP}). All the properties (with subscript l) of the sensible heat transfer in the Eq. (42) are determined based on the bulk fluid in the subcooled state, and the equilibrium thermodynamic quality (x_b) in Eqs. (8)-(12) is replaced by the superficial thermodynamic quality (x_{sup}) which is obtained by Eqs. (16)-(19).

$$\left\{\begin{aligned} \alpha_{SP} &= 0.023\cdot Re_l^{0.8}\cdot Pr_l^{0.4}\cdot\frac{\lambda_l}{d_i} \\ Re_l &= \frac{G_r\cdot(1-x_{sup})\cdot d_i}{\mu_l} \end{aligned}\right. \tag{42}$$

A sensitivity analysis of the effect on the HTC of the Weber number, Jakob number, Bond number, Strouhal number, subcooling degree, and wall temperature, respectively, was conducted in order to identify the more relevant parameters to include in the two correction factors. It was found that the HTC of the sensible and the latent heat transfer components depend significantly on the subcooling degree ($T_{l,sat}$ - T_b). Therefore, the subcooling degree is included in the correction factor of the sensible term (F_{SP}) and the latent term (F_{TP}). Moreover, the wall temperature on the refrigerant side (T_{wr}) is considered in the sensible heat transfer, as the temperature gradient between the fluid and the wall determines the mean fluid properties of the cross-section. The coefficients and power exponents of the correction factors were determined using the least squares method. Around 70 % of the experimental data in the CSC region was used to tune the correlations based on linear regression, finding the best-fitting curve by minimizing the sum of residuals between the data points and the curve. The final equations of these two correction factors are as follows:

Table 1
Key parameters, limitations and applications of the prediction methods under consideration.

Author	Prediction method	Critical parameters	Application(s)
Agarwal et al. [12]	CSH: Eqs. (6) - (12)	Re_v; Pr_v; Re_{lo}; $Pr_{l,sat}$; J_G; J_G^T; ΔT_{sup}; $\Delta T_{sub,w}$; $\Delta T_{b,w}$; λ_v; $\lambda_{l,sat}$; x_b; $\rho_{l,sat}$; ρ_v; $\mu_{l,sat}$; μ_v; g; Δh_{lv}	Horizontal smooth tube $Re_{eq,CSH}$*: 13563–21301 $Re_{eq,TP}$: 4388–17679 $Re_{eq,CSC}$: 4497–7703 Working fluids: R1234ze(E), R134a, and R32
	TP and CSC: Eqs. (8) - (12)	Re_{lo}; $Pr_{l,sat}$; J_G; J_G^T; $\lambda_{l,sat}$; x_b; $\rho_{l,sat}$; $\rho_{v,sat}$; $\mu_{l,sat}$; $\mu_{v,sat}$; g; Δh_{lv}; $\Delta T_{sub,w}$	
Kondou et al. [11]	CSH: Eq. (6) Eqs. (13) - (15)	Re_v; Pr_v; $Re_{l,f}$; $Pr_{l,f}$; J_G; J_G^T; ΔT_{sup}; $\Delta T_{sub,w}$; $\Delta T_{b,w}$; T_{wi}/T_b; λ_v; $\lambda_{l,sat}$; x_b; $\rho_{l,sat}$; $\rho_{v,sat}$; $\mu_{l,sat}$; $\mu_{v,sat}$; $\lambda_{l,f}$; $\rho_{l,f}$; g; Δh_{lv}; $\mu_{l,f}$	Horizontal smooth tube $Re_{eq,CSH}$: 24726–38552 $Re_{eq,TP}$: 17874–36189 $Re_{eq,CSC}$: 19403–19780 Working fluids: R410A and CO_2
	TP: Eqs. (14) - (15)	$Re_{l,f}$; $Pr_{l,f}$; J_G; J_G^T; $\lambda_{l,sat}$; x_b; $\rho_{l,sat}$; $\rho_{v,sat}$; $\mu_{l,sat}$; $\mu_{v,sat}$; $\lambda_{l,f}$; $\rho_{l,f}$; g; Δh_{lv}; $\mu_{l,f}$; $\Delta T_{sub,w}$	
	CSC: Eq. (13)	Re_l; Pr_l; λ_l; T_{wi}; T_b	
Xiao et al. [16]	CSH: Eq. (32) Eq. (23)	$Re_f = f(G, x_{sup}, \mu_{l,sat}, d_i, \rho_{l,sat}, \rho_v, g, \sigma)$; $Pr_{l,sat}$ $\delta = f(G, x_{sup}, \mu_{l,sat}, d_i, \rho_{l,sat}, \rho_v, g, \sigma)$; $\lambda_{l,sat}$; $\Delta T_{sub,w}$; $\Delta T_{b,w}$; $\mu_{l,sat}$; $\mu_{v,sat}$; $\rho_{l,sat}$; $\rho_{v,sat}$; g; σ; x_{sup}	Horizontal smooth tube Mass flux: (100 to 200) $kg{\cdot}m^{-2}{\cdot}s^{-1}$ Hest flux: (5 to 25) $kW{\cdot}m^{-2}$ Working fluids: R1234ze(E), R134a, R32, R410A, and R744
	TP: Eq. (33) Eq. (23)	$Re_f = f(G, x_{sup}, \mu_{l,sat}, d_i, \rho_{l,sat}, \rho_v, g, \sigma)$; $Pr_{l,sat}$ $\delta = f(G, x_{sup}, \mu_{l,sat}, d_i, \rho_{l,sat}, \rho_v, g, \sigma)$; $\lambda_{l,sat}$; $\mu_{l,sat}$; $\mu_{v,sat}$; $\rho_{l,sat}$; $\rho_{v,sat}$; g; σ; x_{sup}	
	CSC: Eq. (33) Eq. (23)	$Re_f = f(G, x_{sup}, \mu_l, d_i, \rho_l, \rho_{v,sat}, g, \sigma)$; Pr_l $\delta = f(G, x_{sup}, \mu_l, d_i, \rho_l, \rho_{v,sat}, g, \sigma)$; λ_l; $\mu_{l,sat}$; $\mu_{v,sat}$; $\rho_{l,sat}$; $\rho_{v,sat}$; g; σ; x_{sup}	
Jacob et al. [10]	CSH: Eqs. (34) - (36) Eq. (7) Eqs. (8) - (12)	Re_v; Pr_v; Re_{lo}; $Pr_{l,sat}$; J_G; J_G^T; ΔT_{sup}; q_{total}; x_{sup}; $c_{p,v}$; ΔT_{glide}; Δh_{lv}; λ_v; $\lambda_{l,sat}$; $\rho_{l,sat}$; $\rho_{v,sat}$; $\mu_{l,sat}$; $\mu_{v,sat}$; g; $\Delta T_{sub,w}$	Horizontal smooth tube $Re_{eq,CSH}$: 10089–88959 $Re_{eq,TP}$: 4561–80069 $Re_{eq,CSC}$: 4036 – 57,253 Working fluids: R448A, R450A, R452A, R454B, and R454C
	TP: Eq. (34) Eq. (7) Eqs. (8) - (12)	Re_{lo}; $Pr_{l,sat}$; J_G; J_G^T; x_{sup}; $c_{p,v}$; ΔT_{glide}; Δh_{lv}; $\lambda_{l,sat}$; $\rho_{l,sat}$; $\rho_{v,sat}$; $\mu_{l,sat}$; $\mu_{v,sat}$; g; $\Delta T_{sub,w}$	
	CSC: $Re \geq 10^4$: Eq. (7) $2300 < Re < 10^4$: Eq. (39) $Re \leq 2300$: Constant wall temperature: Eq. (37) Constant heat flux: Eq. (38)	Re_l; Pr_l λ_l; T_{wi}; T_b	
Longo et al. [8]	CSH and TP: Eq. (40)	$Pr_{l,sat}$; Re_v; Pr_v ΔT_{sup}; $\Delta T_{sub,w}$; $\Delta T_{b,w}$; $c_{p,v}$; Δh_{lv}; G; x_b; $\rho_{l,sat}$; $\rho_{v,sat}$; $\mu_{l,sat}$; $\lambda_{l,sat}$; λ_v	Brazed PHE Re_v:50–15000 $Re_{eq} < 50000$ Working fluids: R134a

* The equivalent Reynolds number (Re_{eq}) is computed by Eq. (40), where the thermodynamic quality x_b is replaced by the superficial quality x_{sup} (obtained from Eqs. (16)-(19)).

$$\begin{cases} F_{SP} = 0.01 \cdot \left(\dfrac{T_{l,sat} - T_b}{T_{wr}}\right)^{4.008} \\ F_{TP} = 0.819 \cdot \left(\dfrac{T_{l,sat} - T_b}{T_{l,sat}}\right)^{0.023} \end{cases} \tag{43}$$

3.8. Uncertainty analysis

The uncertainties of the relevant parameters, including the HTC, the incipience temperature and completion temperature of non-equilibrium condensation, are evaluated using the Kline and McClintock method [27]:

$$u_y = \sqrt{\sum_{k=1}^{n} \left(\frac{\partial y_k}{\partial z_k}\right)^2 u(z_k)^2} \qquad y = f(z_1, z_2, z_3, \ldots, z_n) \tag{44}$$

where $u(z_1)$, $u(z_2)$, …, $u(z_n)$, represent the uncertainties of the direct measurements (including temperatures, pressures, mass flow rates of refrigerants, volume flow rate of secondary fluids), which are provided in the Refs. [13,14,28]. y is a certain calculated parameter, which is determined by direct measurements (z_1, z_2, …, z_n). f is the function relationship between a certain calculated parameter and direct measurements.

The uncertainties of the calculated parameters were calculated using coverage factor K = 2. The results suggest that the uncertainty of the HTC of the refrigerant, incipience temperature, and completion temperature ranges from 2.8 % to 48 %, 1.5 K to 6.8 K, and 0.5 K and 2.3 K, respectively.

4. Evaluation of the prediction methods

4.1. Data collection

In order to evaluate the predictive performance of the prediction methods of non-equilibrium condensation, experimental data available in the open literature were compiled. Table 2 presents the database of non-equilibrium condensation heat transfer in a tube. The database includes data for non-equilibrium condensation, including the CSH, TP and CSC regions. Only the in-tube flow data were found to be adequate for the evaluation of prediction methods. In practice, measuring local heat transfer parameters is much easier in tubular heat exchangers than in heat exchangers with more complex geometry (e.g. PHEs or microchannel heat exchangers). The experimental data in Agarwal [13] and Kondou [14,15] were compiled using the data collection software Engauge Digitizer, while Jacob provided online access to their experimental data [29–32]. All the experimental data were obtained for heat transfer in a tube with a diameter ranging from 4.7 mm to 6.1 mm, and a length ranging from 0.15 m to 1.3 m. The database includes 1119 heat transfer data points. 204 of the data points are located in the CSH region, while 806 and 109 data points are located in the TP region and CSC region, respectively. The classification of the data points is based on the temperature at the incipience point (T_{inc}) and completion point (T_{com}) of the non-equilibrium condensation, which are calculated by Eq. (17) and Eq. (19), respectively. Data with temperature between the incipience temperature and saturation vapor temperature are classified to the CSH region, while those data with a temperature between the saturation liquid temperature and completion temperature are classified to the CSC region. Data with a temperature between the saturation vapor point and saturation liquid point are classified to the TP region.

The working fluids used in the experiments include pure refrigerants (R1234ze(E), R134a, R32 and CO_2) and zeotropic mixtures (R410A, R404A, R454C, R454B, R452A, and R450A). The data from Agarwal [13] and Kondou [14,15] are quasi-local measurements obtained for a 0.15 m test section. As for the data from Jacob [29–32], thermocouples

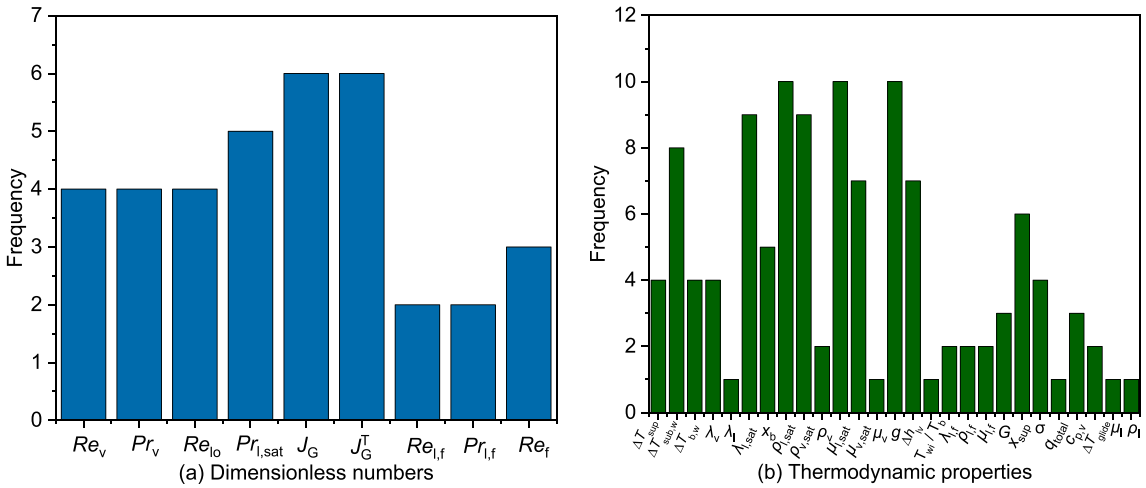

Fig. 4. Frequency of different parameters occurring in the prediction methods under consideration: (a) Dimensionless numbers, (b) Thermodynamic properties.

Table 2
Experimental data of non-equilibrium condensation heat transfer in a tube.

Sources	Tube geometries	Working fluids	Data type	Conditions					Number of data points		
				G ($kg{\cdot}m^{-2}{\cdot}s^{-1}$)	ΔT_{sup} (°C)	ΔT_{sub} (°C)	P_{con} (MPa)	q ($kW{\cdot}m^{-2}$)	CSH	TP	CSC
Agarwal et al. [13]	ID*: 6.1	R1234ze(E)	Quasi-local	100	42	20	1.0	10	6	12	5
	TL*: 150	R134a	Quasi-local	100	32	21	1.3	10	4	10	3
		R32	Quasi-local	100	31	15	3.1	10	6	12	1
Kondou et al. [14,15]	ID: 6.1	R410A	Quasi-local	200	23–33	0	2.7	3.2–22.1	24	19	0
	TL: 150	CO2	Quasi-local	150	17–26	1	6–7	8.8–11.1	17	34	2
Jacob et al. [29–32]	ID: 4.7	R454C	Quasi-local	95–506	6–53	2–34	1.6–2.6	1.2–136.5	51	207	28
	TL: 1300	R454B	Quasi-local	95–504	5–39	3–33	2.2–3.6	0.2–150.9	38	151	18
		R452A	Quasi-local	103–799	9–43	1–23	1.8–2.9	0.2–205.7	17	104	12
		R404A	Quasi-local	102–801	15–39	2–24	1.8–2.9	0.1–204.5	12	52	12
		R134a	Quasi-local	206–596	11–21	3–19	1.1–1.5	6.0–113.2	9	99	16
		R450A	Quasi-local	98–559	7–44	3–26	1.0–1.3	1.2–135.5	20	106	12

* ID and TL represent the inner diameter and total length of the tube, measured in millimeters.

were distributed along the tube to obtain the local temperature of the wall and secondary fluid. The mass flux varies from 95 $kg{\cdot}m^{2}{\cdot}s^{-1}$ to 801 $kg{\cdot}m^{2}{\cdot}s^{-1}$. The ranges of superheating and subcooling degrees used during the experiments are 5 °C to 53 °C and 0 °C to 34 °C, respectively. The condensation pressure varies from 1 MPa to 7 MPa, and the heat flux ranges from 0.1 $kW{\cdot}m^{-2}$ to 205.7 $kW{\cdot}m^{-2}$.

4.2. Assessment indicators of correlations

The mean absolute percentage error (MAPE) and mean percentage error (MPE) are used to evaluate the predictive performance of heat transfer correlations. They are defined by the Eq. (45) and Eq. (46), respectively:

$$MAPE = \frac{100\%}{N}\sum_{i=1}^{N}\left|\frac{HTC_{exp} - HTC_{pre}}{HTC_{exp}}\right| \tag{45}$$

$$MPE = \frac{100\%}{N}\sum_{i=1}^{N}\left(\frac{HTC_{pre} - HTC_{exp}}{HTC_{exp}}\right) \tag{46}$$

where N represents the number of experimental data, while HTC_{exp} and HTC_{pre} indicate the heat transfer coefficients calculated with experimental measurements and prediction methods, respectively.

$Per_{\pm 20\%}$ and $Per_{\pm 30\%}$ characterize the percentage of data that falls within a certain deviation range, ±20 % and ± 30 %, respectively. They are defined by the Eq. (47) and Eq. (48).

$$Per_{\pm 20\%} = \frac{N_{\pm 20\%}}{N} \tag{47}$$

$$Per_{\pm 30\%} = \frac{N_{\pm 30\%}}{N} \tag{48}$$

where $N_{\pm 20\%}$ and $N_{\pm 30\%}$ indicate the amount of the data that falls within the ± 20 % and ± 30 % deviation, respectively. N is the total number of the data points.

4.3. Evaluation of the prediction methods

Generally, a prediction method of a heat transfer process is developed based on certain operation conditions, working fluid(s), heat exchanger type and measurement technique. Therefore, a prediction method may not be applicable for conditions other than those used to obtain the method. In this section, the predictive performance of the four prediction methods (except the Xiao correlation, which will be clarified later) developed for non-equilibrium condensation outlined in Section 3 are assessed by comparing their predictions with the experimental results compiled in Table 2. The possibility of extending the prediction methods to other application areas is explored. In addition, guidance for developing prediction methods with wider application areas and higher accuracy are provided based on the evaluation results.

The predictive performance of the Xiao correlation is not included in this section for a number of reasons. First, in the original model (Eq. (20) – Eq.(31)), as suggested by Xiao et al. [33,34], flow regime maps identifying the transition line between annual and stratified flow are needed

for the implementation of the original model. It is not possible to provide the flow regime maps, because there is no corresponding visualization result from the dataset presented in Table 2. In addition, it is challenging to extend the application area of the flow regime maps from Xiao et al. [33,34] to the present paper due to the different conditions of the analyses. Moreover, the stratification angle (θ_{strat}) of the liquid film in the stratified flow regime is unknown. In terms of the simplified model (Eq. (21) – Eq. (23), Eq. (32) – Eq. (33)), the whole non-equilibrium condensation process is regarded as annual flow, neglecting the effect of gravity on the liquid film. However, this approximation method is only valid in microchannel flow (where the gravity is negligible) or for operating conditions of large mass flux (where the shear force typically dominates). The dataset used in the present paper to evaluate the predictive performance of the correlations applies to heat transfer in a conventional tube with a wide range of mass fluxes, which does not agree with the conditions of the approximation method (microchannel heat transfer and large mass flux). For these reasons, it would not be appropriate to include the Xiao correlation in the analysis presented in this section.

As the different correlations were developed for different regions, including the CSH, TP and CSC regions, the data are also divided into CSH, TP and CSC regions. In order to determine the incipience and completion point of non-equilibrium condensation, Xiao et al. [16] suggested calculating the temperature of incipience and the completion point through iteration using an appropriate prediction method for single-phase heat transfer. Eq. (17) and Eq. (19) were developed for this purpose. In the method, the vapor/liquid saturation temperature, local heat flux, and HTC at incipience and completion points, should be known a priori or be obtained through iteration. However, the heat flux at incipience and completion points cannot be obtained, since the locations of the incipience and completion points are unknown. Moreover, the HTC of the incipience and completion points are based on local thermodynamic properties, which are unknown until the incipience/completion points are determined. Therefore, we made the following approximations:

- According to the definition of the condensation incipience point, the non-equilibrium condensation starts when the wall temperature drops below the vapor saturation temperature. The point where the wall temperature is closest to the vapor saturation temperature was found among the experimental data, and the heat flux and HTC in this point are taken as q_{inc} and α_{inc}. The incipience point is determined using Eq. (17).
- The point of complete non-equilibrium condensation is difficult to determine according to the definition. Not until the highest temperature in the heat transfer channel drops below the liquid saturation temperature, is the non-equilibrium condensation completed. However, only the bulk temperature of the working fluid is normally readily available through experiments, because it is very challenging to measure the temperatures across a cross-sectional segment of the flow channel. For this reason, it was assumed that the first segment, right after the last segment of the TP region, belongs to the CSC

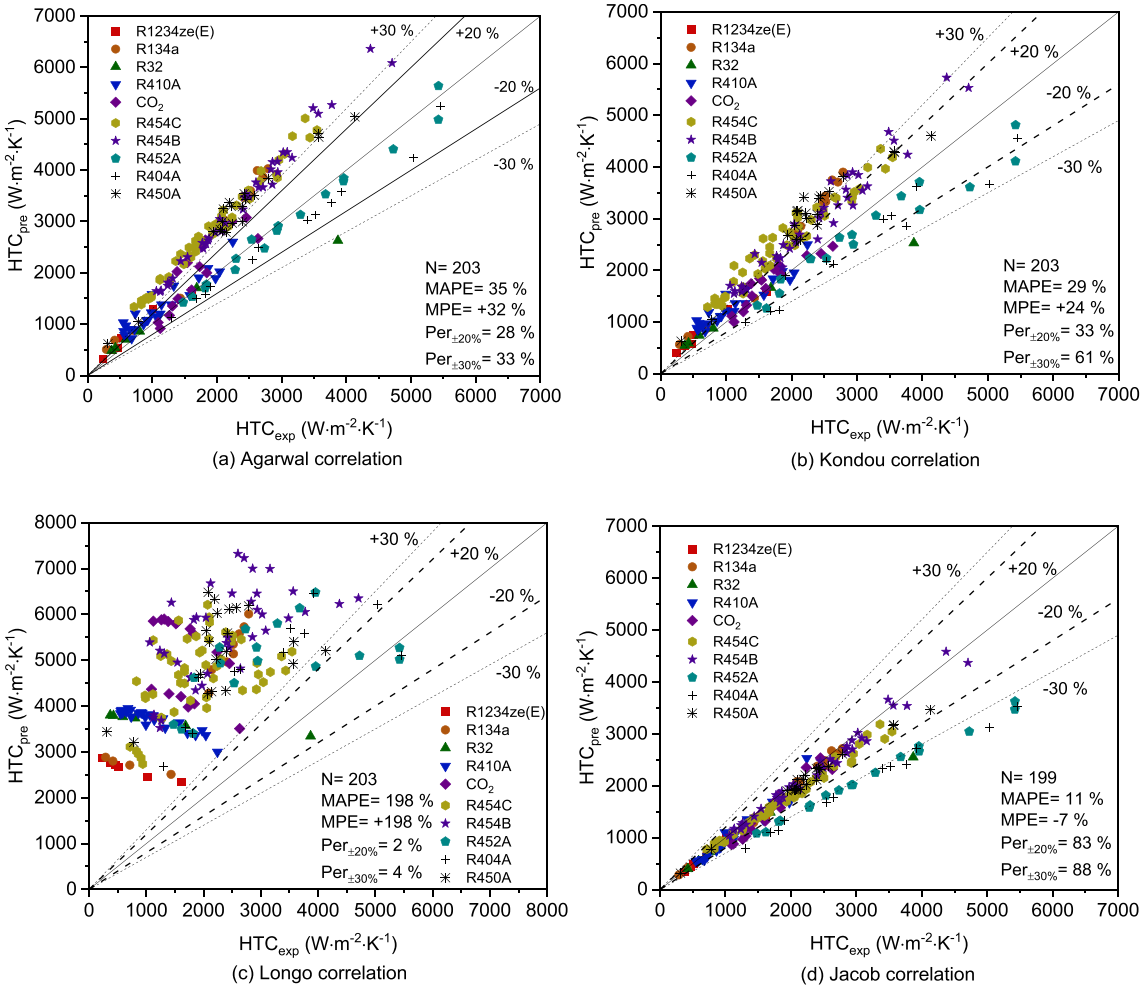

Fig. 5. Comparison of the HTC in the CSH region obtained from prediction methods and experimental data: (a) Agarwal correlation, (b) Kondou correlation, (c) Longo correlation and (d) Jacob correlation.

region. The heat flux and HTC of this segment are regarded as the heat flux (q_{com}) and HTC (α_{com}) of the condensation completion point. In this way, the point of complete condensation is calculated by Eq. (19).

4.3.1. Desuperheated condensation

Fig. 5 presents the HTC obtained using the four prediction methods and experimental data in the CSH zone. In Fig. 5(a), 203 data points in the CSH region are predicted using the Agarwal correlation. The MAPE and MPE of the Agarwal correlation are 35 % and + 32 %, respectively. 28 % of the experimental data are located within ± 20 % deviation, while 33 % of the experimental data are within ± 30 % deviation. The Agarwal correlation is more accurate when predicting the HTC of pure working fluids (R1234ze(E), R134a, R32, CO_2) than that of zeotropic mixtures (R454C, R454B and R450A). The results indicate that the HTC of zeotropic mixtures with a large temperature glide (R454C and R454B) is overestimated. The main reason is that the temperature glide and mass transfer of zeotropic mixtures are not considered in the prediction method. These mixtures effects tend to increase the heat transfer resistance, deteriorating the non-equilibrium condensation [35,36].

As for the Kondou correlation, the results suggest that the MAPE and MPE are reduced to 29 % and + 24 %, respectively, as shown in Fig. 5 (b). 33 % of the data are within ± 20 % deviation, and 61 % of the data are within ± 30 % deviation. The reasons for the improved predictive performance compared with the Agarwal correlation are that it considers the temperature of the condensed film and the wall temperature in the Δ T-independent regime. The effect of improved accuracy due to the inclusion of the wall temperature is shown particularly for the data presented in Jacob [10,28], which have relatively high wall subcooling. However, the correlation overestimates the HTC for zeotropic mixtures, as it does not consider mixture effects.

As indicated in Fig. 5(c), the Longo correlation overestimates the data in the CSH region. The MAPE and MPE are near 200 %, while only 2 % of the 203 data points are within ± 30 % deviation. The Longo correlation has the same format as the Webb model [19], simplifying the temperature difference along the whole CSH region to ($T_{v,sat}$ - T_{wi}). The basic form of the correlation is $\alpha_{CSH}\cdot(T_{v,sat} - T_{wi}) = \alpha_{TP}\cdot(T_{v,sat} - T_{wi}) + \alpha_{SH}\cdot(T_b - T_{wi})$. However, the actual temperature difference of the whole CSH process should be (T_b - T_{wi}), which is larger than that in the simplified model, resulting in the following basic form of the correlation: $\alpha_{CSH}\cdot(T_b - T_{wi}) = \alpha_{TP}\cdot(T_{v,sat} - T_{wi}) + \alpha_{SH}\cdot(T_b - T_{wi})$. In the Longo correlation, the decrease of the heat transfer temperature difference leads to a larger HTC. This is the main reason for the overestimation of the Longo prediction method. Especially in the beginning of the CSH region (namely, small experimental HTC values), the overestimation is significant because the temperature difference T_b - T_{wi} is much larger than the temperature difference $T_{v,sat}$ - T_{wi} in this region.

In addition, it needs to be stressed that the Longo correlation is the only prediction method among the four developed for PHEs. Therefore, it was not intended to be used for the in-tube heat transfer considered in the evaluation presented here. Further research on non-equilibrium condensation in PHEs is required, covering both fundamental research analyzing the heat transfer mechanisms and prediction methods to be used for design, modelling and optimization of condensers including desuperheating and subcooling.

Among the four correlations, the results suggest that the Jacob correlation gives the most accurate prediction for the CSH region. The MAPE and MPE are 11 % and −7 %, respectively, as shown in Fig. 5(d). 83 % of the data points are located within ± 20 % deviation, and 88 % of the data points are located within ± 30 % deviation. Interestingly, the Jacob correlation depends on the estimation of the superficial thermodynamic quality. However, it is challenging to determine the completion point of non-equilibrium condensation using the local heat flux and HTC. Therefore, in order to improve further the accuracy of the Jacob correlation, we propose to develop new methods for the determination of the completion point for the target heat transfer.

4.3.2. Saturated two-phase condensation

Fig. 6 presents the HTC obtained using the four prediction methods and 806 experimental data points in the TP zone. Fig. 6(a) indicates that the MAPE and MPE are 20 % and + 17 %, respectively, for the Agarwal correlation. 57 % of the data are located within ± 20 % deviation, and 83 % of the data are located within ± 30 % deviation. The correlation achieves a higher accuracy for the dataset of Agarwal [13] and Kondou [14,15] (with low wall subcooling degree) than for that of Jacob [29–32] (with high wall subcooling degree). The main reason for the accuracy difference is that the wall temperature is not taken into account in the Δ T-independent regime, causing larger deviations for high wall subcooling conditions. In addition, the mixture effects of zeotropic mixtures are not considered.

The Kondou correlation attains the highest accuracy, compared to other prediction methods. As shown in Fig. 6(b), the correlation has an MAPE of 11 % and an MPE of +1 %. 87 % of the data are located within ± 20 % deviation, and only 5 % of the data have a deviation larger than ± 30 %. The Kondou correlation had the same basic format as the Agarwal correlation, but introduced the wall subcooling degree to the Δ T-independent regime, which the Agarwal correlation does not include. Compared to the Agarwal correlation, the Kondou correlation achieves better predictive performance, especially for the Jacob dataset (with larger wall subcooling). The results suggest that the wall subcooling has a strong influence on the HTC in the Δ T-independent regime, especially for large wall subcooling conditions. Furthermore, the results indicate that the Kondou correlation works well for zeotropic mixtures (refer to the results of the fluids R454C, R454B and R450A), indicating that the film theory reflects the mixture effects well.

The Longo correlation applied to the TP region is based on the Dittus-Boelter equation [23], by modifying the multipliers and indexes of the Reynolds number and Prandtl number to improve the accuracy of the correlation. In addition, as pointed out previously, Longo et al. [8] developed the correlation for PHEs rather than for in-tube heat transfer. For these reasons, it is not surprising that the Longo correlations cannot predict the in-tube heat transfer data with high accuracy. According to the results shown in Fig. 6(c), the experimental data are overestimated, having an MAPE and MPE of 47 % and + 45 %, respectively. More than half of the data have a deviation larger than ± 30 %.

The results suggest that the Jacob correlation provides the second-best predictive performance, after the Kondou correlation. According to the results shown in Fig. 6(d), the Jacob correlation has an MAPE and MPE of 12 % and −4 %, respectively. 85 % of the experimental data are located within ± 20 % deviation, and less than 5 % of the data have a deviation greater than ± 30 %. Compared to the results of the Agarwal correlation, the MAPE increases by 8 % after introducing the SBG method. However, it is worth noting that the Cavallini model [21] with the SBG method achieves good predictive performance for both pure working fluids and zeotropic mixtures in the TP region.

4.3.3. Subcooled condensation

Kondou et al. [11] and Jacob et al. [10] simplified the CSC region to single-phase heat transfer and applied the Gnielinski model [20] to predict the HTC. On the contrary, Agarwal et al. [12] considered the phase change heat transfer in this region and developed a corresponding correlation. There is no corresponding correlation for the CSC region in the Longo model.

Fig. 7 presents the HTC obtained using the three prediction methods and 109 experimental data points in the CSC region. The results shown in Fig. 7(a) - (b) indicate that the Kondou and Jacob correlations provide acceptable predictive performance when using single-phase correlations to predict the data in the CSC region. The MAPEs of these two correlations are smaller than 30 %. More than 65 % of the data points are located within ± 30 % deviation, while almost 56 % of the data points are located within ± 20 % deviation. However, both the correlations

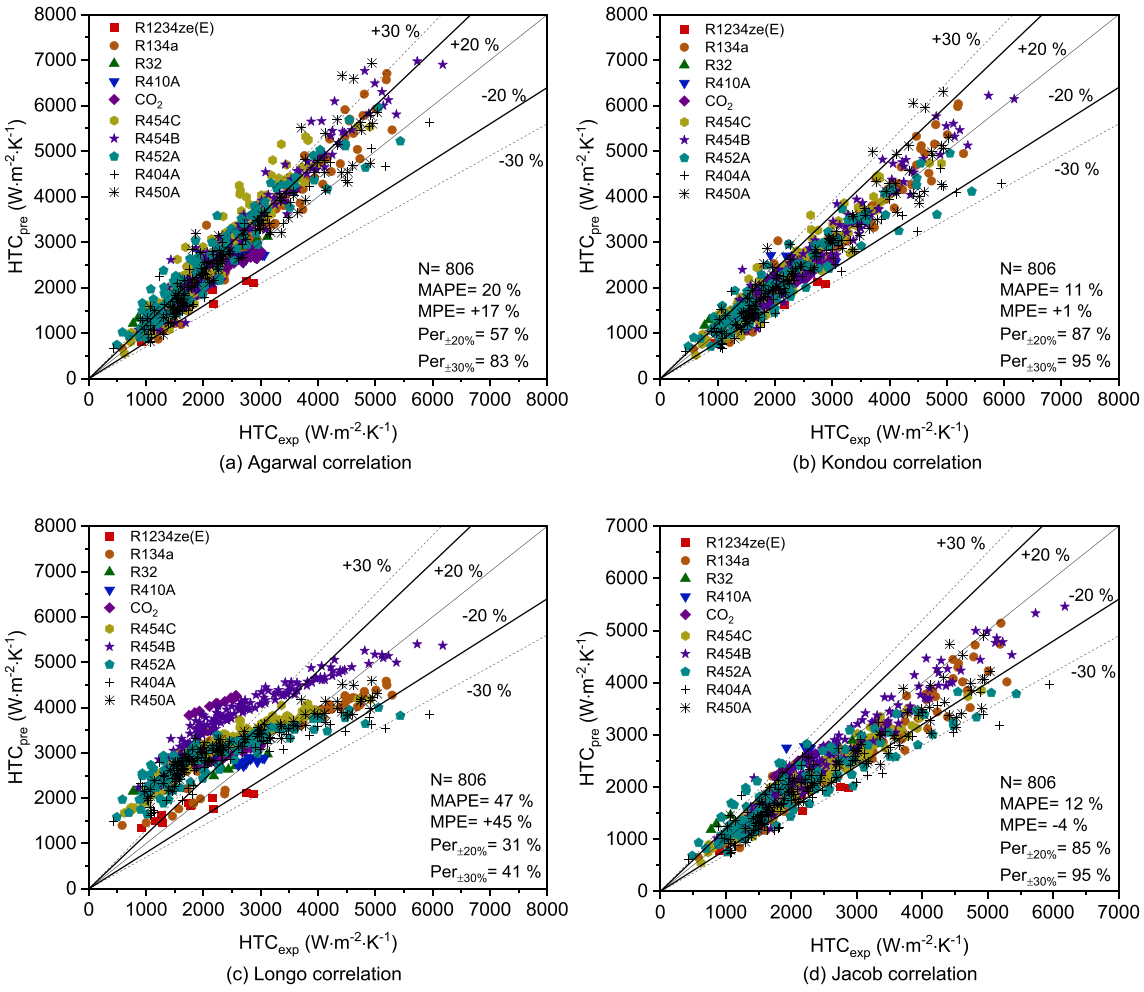

Fig. 6. Comparison of the HTC in the TP region obtained using the prediction methods and experimental data: (a) Agarwal correlation, (b) Kondou correlation, (c) Longo correlation and (d) Jacob correlation.

underestimate the HTC in the CSC region, resulting in negative MPEs (around −15 %). That is, the HTC in the CSC region is underestimated when neglecting the effect of two-phase heat transfer in the CSC region. Therefore, in order to improve the accuracy of prediction methods for the CSC region, there is a need to investigate the heat transfer mechanisms and to develop new prediction methods incorporating the effect of two-phase heat transfer in this region.

As indicated in Fig. 7(c), the MAPE and MPE of the Agarwal correlation are 43 % and + 43 %, respectively. 54 % of the data are located within ± 30 % deviation, and 30 % of the data are located within ± 20 % deviation. The results suggest that the Agarwal correlation overestimates the HTC in the CSC region. The reason is that only the two-phase heat transfer was considered in the CSC region, using the classic two-phase correlation proposed by Cavallini [21] to predict the HTC. However, in practice both single-phase and two-phase heat transfer take place in the CSC region simultaneously. In addition, the completion point of the CSC region was determined using Eq.(19), implying that the local heat flux and HTC at the completion point were replaced by those of the first segment of the CSC region. Therefore, it is critical to develop a new prediction method to determine the completion point for non-equilibrium condensation.

Table 3 lists the assessment indicators to compare the predictive performance of the four methods developed for non-equilibrium condensation heat transfer. The Jacob prediction method has the best predictive performance, with an MAPE of 13 % and an MPE of −6.4 %. More than 91 % of the data have a deviation within ± 30 %, and about 82 % of the data points are located within ± 20 % deviation. The Kondou prediction method has the second-best predictive performance, with an MAPE near 15 % and 87 % of the data points located within ± 30 % deviation. The Agarwal correlation also has acceptable predictive performance for non-equilibrium condensation, with an MAPE of 25 % and about 71 % of the data points within ± 30 % deviation. The results suggest that the Xiao and Longo methods fail to predict the data of non-equilibrium condensation heat transfer inside a tube.

Fig. 8(a) presents the result of the tuning of the new correlation based on 70 % of the data, while Fig. 8(b) presents the validation results of the correlation based on the rest of the data (30 %); the latter serving as an evaluation of the correlation's predictive performance. While Fig. 8(a) presents results for the fluids R1234ze(E), R134a, R32, CO_2, R454C, R404A, and R450A, Fig. 8(b) presents results for the fluids R454B and R454A.

The results shown in Fig. 8(a) indicate that the proposed correlation is in fair agreement with the experimental data, with a MAPE of 14 % and a MPE of + 4 %. More than three-fourths of the data falls within the ± 20 % deviation, while around 90 % of the data is located within the ± 30 % deviation. The validation results presented in Fig. 8(b) indicate that the proposed correlation can be applied with reasonable accuracy also to other refrigerants that the ones used to tune the correlation, achieving a MAPE of 12 % and a MPE of + 4 %. Moreover, 87 % of the data is within the deviation range of ± 20 %. The proposed model reduces the MAPE by more than 8 %-points, from 20 % to 12 %, compared with the correlation attaining the best accuracy considered in the paper, the Kondou correlation [11], see Fig. 7.

Table 4 presents the results of the predictive performance in the low

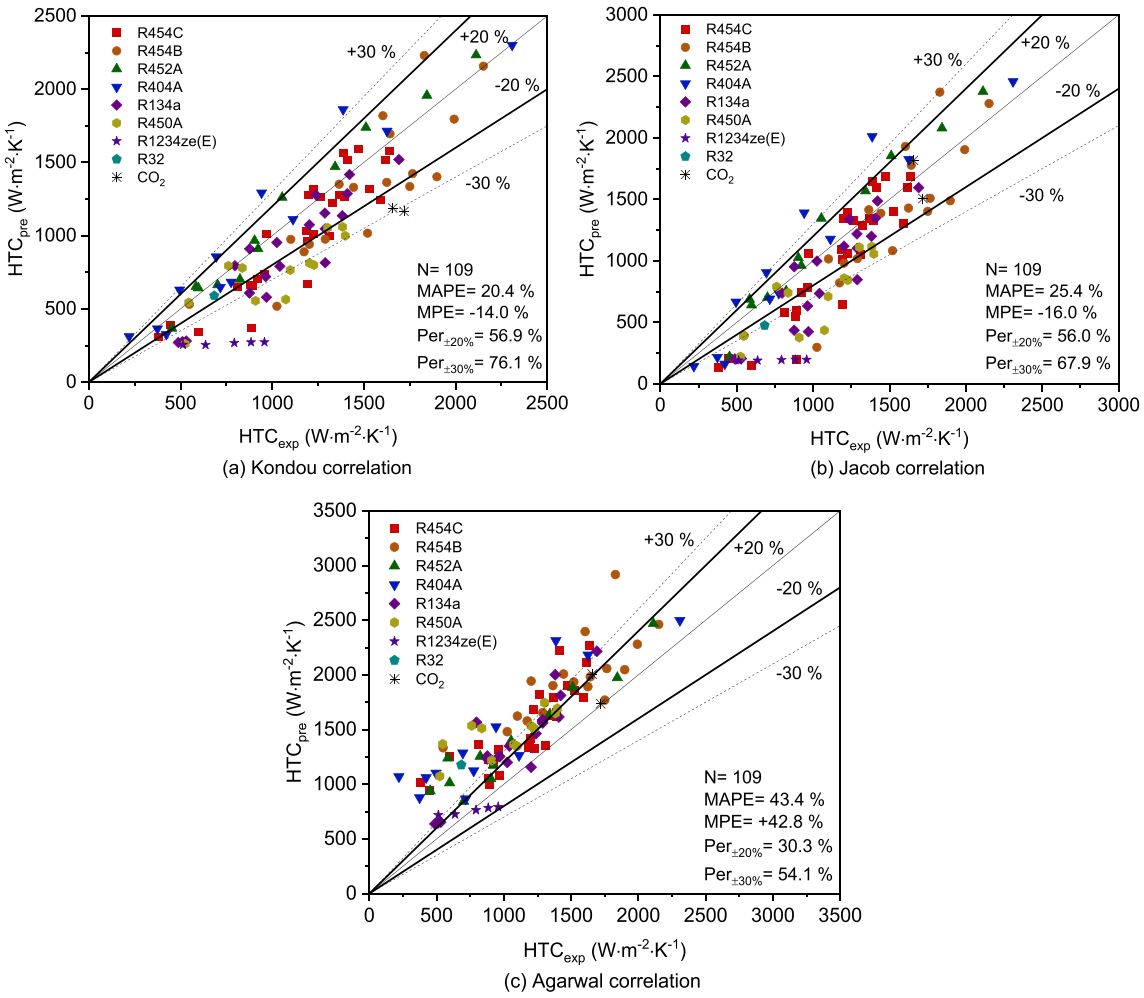

Fig. 7. Comparison of HTC in the CSC region obtained from prediction methods and experimental data: (a) Kondou correlation, (b) Jacob correlation and (c) Agarwal correlation.

Table 3
Comparison of the predictive performance of the four correlations developed for non-equilibrium condensation heat transfer.

Prediction method	MAPE (%)	MPE (%)	$Per_{\pm 20\%}$(%)	$Per_{\pm 30\%}$(%)
Agarwal et al. [12]	24.6	+22.4	49.4	71.0
Kondou et al. [11]	14.9	+3.7	74.4	87.1
Jacob et al. [10]	12.8	−6.4	82.0	91.4
Longo et al. [8]	77.7	+75.8	25.2	33.4

HTC region ($HTC_{exp} < 1000$) for the three state-of-the-art correlations and the new prediction method. The results suggest that the new prediction method achieves an improvement in the predictive performance for this region.

5. Conclusions

This paper presented an analysis of the prediction methods for non-equilibrium condensation heat transfer. The heat transfer mechanisms of non-equilibrium condensation were discussed, and state-of-the-art prediction methods developed for the target heat transfer processes were analyzed. A database containing all data available in the open literature was compiled and used to evaluate the predictive performance of the prediction methods. In addition, a new prediction method for the subcooled condensation was developed based on the governed heat transfer mechanisms. The main conclusions of the analysis are the following:

1. The Webb model [19] is commonly utilized as the basic form for the desuperheated condensation region, combining the effects of superheated vapor and two-phase heat transfer on the heat transfer coefficient. The Gnielinski model [20] and Dittus-Boelter equation [23] are widely used for single-phase heat transfer, while the Cavallini model [21] is normally utilized for two-phase heat transfer analyses. When it comes to prediction methods for zeotropic mixtures, the equilibrium Silver, Bell and Ghaly method [24,25] is utilized as the basic format, considering the mixture effects. The same prediction methods are used for the subcooled condensation and two-phase condensation regions. Some researchers neglect the subcooled condensation region, since the heat transfer enhancement effect of the two-phase flow is limited. Essential parameters for the analysis of non-equilibrium condensation include superheating degree, wall subcooling degree, superficial thermodynamic quality, and temperature glide (relevant only for mixtures).
2. Existing prediction methods underestimate the heat transfer coefficient in the subcooled condensation regions due to neglecting the latent heat transfer in this region. The new prediction method proposed for the subcooled condensation region, combining latent and sensible heat transfer, achieves a bit better agreement with the experimental data (mean absolute percentage error of 12 %) than does the state-of-the-art correlation attaining the best agreement (mean absolute percentage error of 20 %).

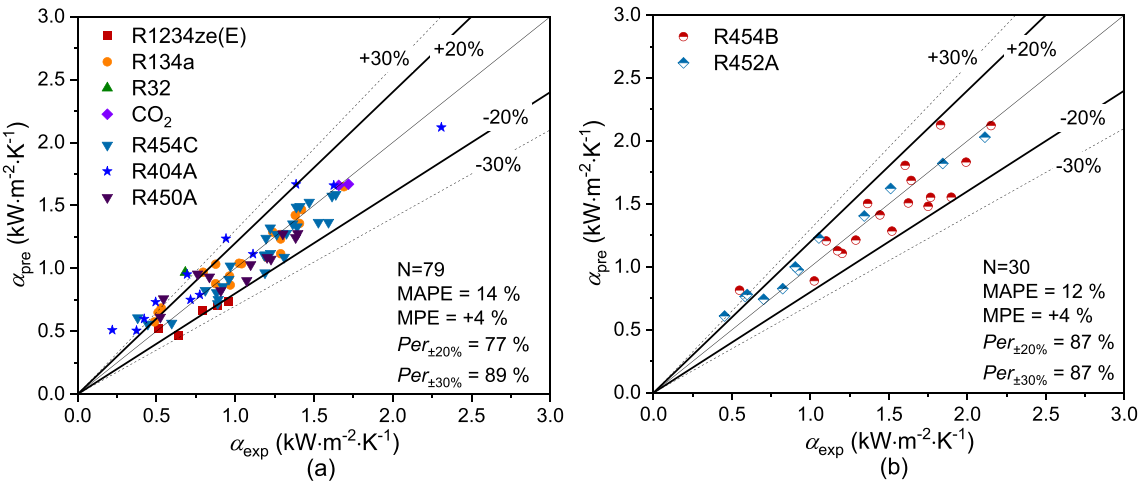

Fig. 8. (a) Tuning results and (b) validation results of the new prediction method.

Table 4
Predictive performance in the low HTC region ($HTC_{exp} < 1000$) for the three state-of-the-art correlations and the new prediction method.

Prediction method	MAPE (%)	MPE (%)	$Per_{\pm 20\%}$(%)	$Per_{\pm 30\%}$(%)
Agarwal et al. [12]	69.1	67.6	17.8	33.3
Kondou et al. [11]	26.0	−18.6	44.4	64.4
Jacob et al. [10]	37.8	−29.9	33.3	40.0
New prediction method	20.0	14.8	53.3	73.3

3. The results suggest that the Jacob prediction method [10] provides the best predictive performance for the desuperheated condensation, with a mean absolute percentage error of 11 %. The Jacob prediction method [10] is recommended to predict the heat transfer coefficient in the desuperheated condensation region. The Kondou prediction method [11] shows good predictability for the saturated two-phase region, with a mean absolute percentage error of 11 %. The Kondou prediction method [11] is suggested to predict the heat transfer coefficient in the saturated condensation region.

As for future research, we suggest to conduct simulation/experimental work to identify the optimal inlet superheating degree and outlet subcooling degree of condensers, maximizing the heat transfer performance of non-equilibrium condensation. Moreover, there is a need to measure local/quasi-local heat transfer coefficients during non-equilibrium condensation in heat exchanger types other than tubes (e.g. plate heat exchangers and microchannel heat exchangers) by means of local heat flux/wall temperature measurement methods or infrared cameras, which would enable the development of appropriate case specific and/or generally applicable prediction methods for non-equilibrium condensation.

CRediT authorship contribution statement

Xiaosheng Zheng: Conceptualization, Methodology, Formal analysis, Investigation, Data curation, Writing – original draft, Funding acquisition. **Ji Zhang:** Conceptualization, Writing – review & editing, Supervision, Funding acquisition. **Martin Ryhl Kærn:** Conceptualization, Writing – review & editing, Supervision. **Fredrik Haglind:** Conceptualization, Writing – review & editing, Supervision, Project administration, Funding acquisition.

Declaration of Competing Interest

The authors declare that they have no known competing financial interests or personal relationships that could have appeared to influence the work reported in this paper.

Data availability

Data will be made available on request.

Acknowledgments

The research carried out by the first author of the paper was funded by the China Scholarship Council [File No. 202008440488]. The financial support is gratefully acknowledged.

References

[1] W.W. Akers, H.A. Deans, O.K. Crosser, Condensing heat transfer within horizontal tubes, Chem. Eng. Prog. Symp. Ser. 55 (1959) 171–176.
[2] International Energy Agency, World Energy Outlook 2022 - Key findings, 2022. https://www.iea.org/reports/world-energy-outlook-2022/key-findings.
[3] International Energy Agency (IEA), Global CO2 emissions rebounded to their highest level in history in 2021, 2022. https://www.iea.org/news/global-co2-emissions-rebounded-to-their-highest-level-in-history-in-2021.
[4] X. Yang, J. Xu, Z. Miao, J. Zou, C. Yu, Operation of an organic Rankine cycle dependent on pumping flow rates and expander torques, Energy 90 (2015) 864–878, https://doi.org/10.1016/j.energy.2015.07.121.
[5] G. Pottker, P. Hrnjak, Effect of the condenser subcooling on the performance of vapor compression systems, Int. J. Refrig. 50 (2015) 156–164, https://doi.org/10.1016/j.ijrefrig.2014.11.003.
[6] K. Sarraf, S. Launay, L. Tadrist, Analysis of enhanced vapor desuperheating during condensation inside a plate heat exchanger, Int. J. Therm. Sci. 105 (2016) 96–108, https://doi.org/10.1016/j.ijthermalsci.2016.03.001.
[7] Z. Zhao, Y. Li, L. Wang, K. Zhu, F. Xie, Experimental study on film condensation of superheated vapour on a horizontal tube, Exp. Therm. Fluid Sci. 61 (2015) 153–162, https://doi.org/10.1016/j.expthermflusci.2014.10.029.
[8] G.A. Longo, Refrigerant R134a condensation heat transfer and pressure drop inside a small brazed plate heat exchanger, Int. J. Refrig. 31 (2008) 780–789, https://doi.org/10.1016/j.ijrefrig.2007.11.017.
[9] M. Goto, H. Hotta, S. Tezuka, Film condensation of refrigerant vapours on a horizontal tube, Int. J. Refrig. 3 (1980) 161–166, https://doi.org/10.1016/0140-7007(80)90097-3.
[10] T.A. Jacob, B.M. Fronk, A heat transfer model to predict superheated and saturated condensation of HFC/HFO refrigerant mixtures, Int. J. Heat Mass Transf. 170 (2021), 120947, https://doi.org/10.1016/j.ijheatmasstransfer.2021.120947.
[11] C. Kondou, P. Hrnjak, Heat rejection in condensers close to critical point-de-superheating, condensation in superheated region, and condensation of two-phase fluid, Heat Transf. Eng. 34 (2013) 1180–1190, https://doi.org/10.1080/01457632.2013.776883.
[12] R. Agarwal, P. Hrnjak, Effect of sensible heat, condensation in superheated and subcooled region incorporated in unified model for heat rejection in condensers in horizontal round smooth tubes, Appl. Therm. Eng. 71 (2014) 378–388, https://doi.org/10.1016/j.applthermaleng.2014.05.071.
[13] R. Agarwal, P. Hrnjak, Condensation in two phase and desuperheating zone for R1234ze(E), R134a and R32 in horizontal smooth tubes, Int. J. Refrig. 50 (2015) 172–183, https://doi.org/10.1016/j.ijrefrig.2014.10.015.

[14] C. Kondou, P. Hrnjak, Condensation from superheated vapor flow of R744 and R410A at subcritical pressures in a horizontal smooth tube, Int. J. Heat Mass Transf. 55 (2012) 2779–2791, https://doi.org/10.1016/j.ijheatmasstransfer.2012.01.030.
[15] C. Kondou, P. Hrnjak, Heat rejection from R744 flow under uniform temperature cooling in a horizontal smooth tube around the critical point, Int. J. Refrig. 34 (2011) 719–731, https://doi.org/10.1016/j.ijrefrig.2010.11.003.
[16] J. Xiao, P. Hrnjak, A heat transfer model for condensation accounting for non-equilibrium effects, Int. J. Heat Mass Transf. 111 (2017) 201–210, https://doi.org/10.1016/j.ijheatmasstransfer.2017.03.019.
[17] J. Xiao, P. Hrnjak, Heat transfer and pressure drop of condensation from superheated vapor to subcooled liquid, Int. J. Heat Mass Transf. 103 (2016) 1327–1334, https://doi.org/10.1016/j.ijheatmasstransfer.2016.08.036.
[18] G.A. Longo, G. Righetti, C. Zilio, A new computational procedure for refrigerant condensation inside herringbone-type Brazed Plate Heat Exchangers, Int. J. Heat Mass Transf. 82 (2015) 530–536, https://doi.org/10.1016/j.ijheatmasstransfer.2014.11.032.
[19] R.L. Webb, Convective condensation of superheated vapor, J. Heat Transfer. 120 (1998) 418–421, https://doi.org/10.1115/1.2824266.
[20] V. Gnielinski, Ein neues Berechnungsverfahren für die Wärmeübertragung im Übergangsbereich zwischen laminarer und turbulenter Rohrströmung, Eng. Res. 61 (1995) 240–248.
[21] A. Cavallini, D. Del Col, L. Doretti, M. Matkovic, L. Rossetto, C. Zilio, G. Censi, Condensation in horizontal smooth tubes: A new heat transfer model for heat exchanger design, Heat Transf. Eng. 27 (2006) 31–38, https://doi.org/10.1080/01457630600793970.
[22] B.S. Petukhov, Heat Transfer and Friction in Turbulent Pipe Flow with Variable Physical Properties, Adv. Heat Transf. 6 (1970) 503–564, https://doi.org/10.1016/S0065-2717(08)70153-9.
[23] F.W. Dittus, L.M.K. Boelter, Heat transfer in automobile radiators of the tubular type, Int. Commun. Heat Mass Transf. 12 (1985) 3–22, https://doi.org/10.1016/0735-1933(85)90003-X.
[24] L. Silver, Gas cooling with aqueous condensation, Trans. Inst. Chem. Eng. 25 (1947) 30–42.
[25] K. Bell, M. Ghaly, An approximate generalized design method for multicomponent/partial condenser, Am. Inst. Chem. Eng. Symp. Ser. 69 (1973) 72–79.
[26] B. Thonon, Design method for plate evaporators and condensers, Proc. 1st Int, Conf. Process Intensif. Chem. Ind. BHR Gr. Conf. Ser. Publ. 18 (1995) 37–47.
[27] S.J. Kline, F.A. McClintock, Describing uncertainties in single-sample experiments, Mech. Eng. 75 (1953) 3–8.
[28] T.A. Jacob, B.M. Fronk, In-Tube condensation of zeotropic refrigerant R454C from superheated vapor to subcooled liquid, Sci. Technol. Built Environ. 26 (2020) 1177–1190, https://doi.org/10.1080/23744731.2020.1804281.
[29] T.A. Jacob, B. Fronk, In-tube condensation data of R454B in a horizontal 4.7 mm ID tube, (2020). Doi: 10.6084/m9.figshare.12921407.v1.
[30] T.A. Jacob, E.P. Matty, B. Fronk, In-tube condensation data of R404A, R448A, and R452A in a horizontal 4.7 mm ID tube, (2019). Doi: 10.6084/m9.figshare.10024739.v2.
[31] T.A. Jacob, E.P. Matty, B. Fronk, In-tube condensation data of R134a and R450A in a horizontal 4.7 mm ID tube, (2019). Doi: 10.6084/m9.figshare.7611674.v2.
[32] T.A. Jacob, B. Fronk, In-tube condensation data of R454C in a horizontal 4.7 mm ID tube, (2020). Doi: 10.6084/m9.figshare.12235454.v2.
[33] J. Xiao, P. Hrnjak, A new flow regime map and void fraction model based on the flow characterization of condensation, Int. J. Heat Mass Transf. 108 (2017) 443–452, https://doi.org/10.1016/j.ijheatmasstransfer.2016.11.104.
[34] J. Xiao, Non-equilibrium effects on in-tube condensation from superheated vapor, Ph. D Thesis. (2019) 53–59.
[35] J. Zhang, B. Elmegaard, F. Haglind, Condensation heat transfer and pressure drop characteristics of zeotropic mixtures of R134a/R245fa in plate heat exchangers, Int. J. Heat Mass Transf. 164 (2021), https://doi.org/10.1016/j.ijheatmasstransfer.2020.120577.
[36] X. Huang, J. Zhang, F. Haglind, Experimental analysis of hydrofluoroolefin zeotropic mixture R1234ze(E)/R1233zd(E) condensation in a plate heat exchanger, Int. Commun. Heat Mass Transf. 135 (2022), 106073, https://doi.org/10.1016/j.icheatmasstransfer.2022.106073.